Hindawi
Advances in Meteorology
Volume 2022, Article ID 1926854, 20 pages
https://doi.org/10.1155/2022/1926854

Research Article

Evaluation of Satellite Rainfall Products over the Mahaweli River Basin in Sri Lanka

Helani Perera,[1] Shalinda Fernando,[1] Miyuru B. Gunathilake,[2] T. A. J. G. Sirisena,[3] and Upaka Rathnayake[1]

[1]*Department of Civil Engineering, Faculty of Engineering, Sri Lanka Institute of Information Technology, Malabe, Sri Lanka*
[2]*Division of Hydrology and Aquatic Environment, Environment and Natural Resources, Norwegian Institute of Bioeconomy and Research, Ås, Norway*
[3]*Department of Water Engineering and Management, University of Twente, Enschede, Netherlands*

Correspondence should be addressed to Upaka Rathnayake; upaka.r@sliit.lk

Received 17 December 2021; Accepted 18 March 2022; Published 25 April 2022

Academic Editor: Antonio Donateo

The availability of accurate spatiotemporal rainfall data is of utmost importance for reliable predictions from hydroclimatological studies. Challenges and limitations faced due to the absence of dense rain gauge (RG) networks are seen especially in the developing countries. Therefore, alternative rainfall measurements such as satellite rainfall products (SRPs) are used when RG networks are scarce or completely do not exist. Noteworthy, rainfall data retrieved from satellites also possess several uncertainties. Hence, these SRPs should essentially be validated beforehand. The Mahaweli River Basin (MRB), the largest river basin in Sri Lanka, is the heart of the country's water resources contributing to a significant share of the hydropower production and agricultural sector. Given the importance of the MRB, this study explored the suitability of SRPs as an alternative for RG data for the basin. Daily rainfall data of six types of SRPs were extracted at 14 locations within the MRB. Thereafter, statistical analysis was carried out using continuous and categorical evaluation indices to evaluate the accuracy of SRPs. Nonparametric tests, including the Mann-Kendall and Sen's slope estimator tests, were used to detect the possibility of trends and the magnitude, respectively. Integrated MultisatellitE Retrievals for Global Precipitation Measurement (IMERG) outperformed among all SRPs, while Precipitation Estimation from Remotely Sensed Information using Artificial Neural Networks (PERSIANN) products showed dire performances. However, IMERG also demonstrated underestimations when compared to RG data. Trend analysis results showcased that the IMERG product agreed more with RG data on monthly and annual time scales while Tropical Rainfall Measurement Mission Multisatellite Precipitation Analysis–3B42 (TRMM-3B42) agreed more on the seasonal scale. Overall, IMERG turned out to be the best alternative among the SRPs analyzed for MRB. However, it was clear that these products possess significant errors which cannot be ignored when using them in hydrological applications. The results of the study will be valuable for many parties including river basin authorities, agriculturists, meteorologists, hydrologists, and many other stakeholders.

1. Introduction

Water is being regarded as a remarkable substance due to its critical role related to human life. Reduced precipitation amounts can lead to prolonged droughts while excess precipitation rates can result in flooding. However, both extreme conditions disrupt the socioeconomic activities of people and harm the environment adversely. Water plays an important role in a country's economy in terms of irrigated agriculture, hydropower generation, provision of drinking water, and industrial use [1]. This marks the importance of proper water management for both social and economic benefits for a country. For proper management of water, accurate predictions from hydrological modeling are required. Hence, the role of spatially distributed precipitation data is crucial in this context [2].

Precipitation and evapotranspiration are the major components of the hydrologic cycle, and both these components carry significant shares of the hydrologic cycle [3]. Until the early 1980s, the only method used to obtain these

precipitation data was rain gauges (RGs) located across the world [4]. Although RG data are the most accurate method of measuring rainfall [5], there are significant challenges faced when maintaining rain gauge networks. These challenges are due to complex geographical features, harsh climatological environments, and high financial burdens [6]. Some of the reported shortcomings of RG data are missing rainfall days, data transmission dropouts, calibration errors of the RGs, and local wind effects affecting rainfall level estimations [7, 8]. Incidences during the period of war in countries also lead to collapsing of these rain gauges which ultimately resulted in no rainfall records in certain regions of the world [9].

With the continuous evolvement of science and technology, currently, several other methods are available to obtain rainfall data. They are radars, satellites, and reanalysis products. However, high costs for installment and maintenance of radar networks are unbearable for the developing world to adopt radar networks [6]. On the other hand, reanalysis products have significant biases [10]. Therefore, the satellite rainfall product (SRP) data have grabbed the attention of many researchers due to its ability to provide spatiotemporal rainfall data addressing most of the shortcomings faced when using RGs. The SRPs are attractive since they are available at no cost. In addition, the SRPs are available from fine spatial and temporal scales such as 0.10° and 30 minutes. For instance, both the near-real-time product of GSMaP and IMERG provides 30-minute resolution while the IMERG product provides rainfall in 0.10° resolution [11]. There are many SRPs available and most of them have been used in similar research studies as well. Some of them are Tropical Rainfall Measurement Mission (TRMM), Multisatellite Precipitation Analysis (TMPA) [12], Climate Prediction Center Morphing (CMORPH) [13], Precipitation Estimation from Remotely Sensed Information using Artificial Neural Networks (PERSIANN) [14], and Multisource Weighted Ensemble Precipitation (MSWEP) [15]. But these products have been found to possess inherent systematic uncertainties and sampling errors which need to be clearly studied and identified before using them in hydrological applications [16, 17]. However, for flood and drought predictions, understanding global climate change, and determining the availability of water resources for agriculture and industrial purposes, the climatological data needs to be accurate. Therefore, comparing SRPs by benchmarking with RGs is essential to obtain a sound conclusion on their levels of uncertainty and thereafter to determine their suitability for many practical applications.

Following this requirement, many research studies have been conducted around the world to assess the accuracy and reliability of SRPs with respect to RG data [6, 18–20]. Many studies have demonstrated that TRMM (TMPA) is comparatively better than other SRPs since it used available gauge measurements in its calibration process [21, 22]. Higher efficiency [23] and higher accuracy [24] shown by TRMM 3B42 in research studies had proven its accuracy compared to its near-real-time product (TRMM B42RT). Research studies incorporating CMORPH had observed that it shows dependencies on rainfall estimates [25]. GPM (IMERG) when compared with TMPA in a study conducted in India showed better performance in capturing heavy rainfall events [26]. A study in Ethiopia that focused on CMORPH and PERSIANN-CCS discovered that almost 50% of underestimations can be expected from these SRPs and is cautious to be directly used in flood prediction models [16]. GSMaP-MVK data was proved to produce overestimates when compared with gauge data in a study conducted in Indonesia [27]. Although in the developed world, many studies have been carried out to examine the efficiency of SRPs as an alternative for RGs, the developing region has been least focused in this regard. In the context of Sri Lanka, only a few studies have been carried out to examine the efficiency of SRPs. A previous study was carried out for the Mundeni Aru Basin, Sri Lanka, to evaluate the applicability of SRPs in flood hazard mapping [28]. Two other studies attempted to determine the accuracy of SRPs in streamflow simulation for the Seethawaka watershed, Sri Lanka, using a hydrological model [29, 30].

The Mahaweli River Basin (MRB) in Sri Lanka covers approximately one-sixth of the landmass in the country (Figure 1). The MRB is imperative due to its major role played in hydropower generation and irrigation water supply for many parts of the country. The MRB is the main water supplier for agricultural activities in the eastern dry zone of the country irrigating more than 1,000 km^2 of land. The hydroelectricity produced from six dams of the MRB (Figure 1) supplies more than 40% of the country's electricity. More importantly, all three climatic zones of Sri Lanka fall within the MRB [31, 32]. Despite the vital importance of the MRB to Sri Lanka, the amount of research carried out in this study region is handful. Previously, many studies have been carried out in the subbasins of the MRB and only a very few have focused on the entire MRB. Some of the disciplines which investigated the entire MRB were hydrologic modeling [33], climate change impacts on paddy cultivation in dry zones in the MRB [34], assessing the streamflow variability and rainfall trend of climatic zones [35], El-Nino and La-Nina impact on streamflow [31], drought occurrence and atmospheric circulation [36], and projection of future climate [37]. Other research studies which focused on the subbasins of the MRB investigate the prediction of streamflow in ungauged catchments [38] and flood modeling [39]. Additionally, the Uma-Oya subbasin of the MRB has been an area of great interest for soil erosion. Some of the studies carried out in the Uma-Oya watershed focused on the assessment of the impact of siltation on hydropower generation [40], soil erosion studies [41, 42], land-use change impact on landslides [43], and land-use change impacts on river health [44, 45]. Several field-scale studies have also been conducted to investigate water pollution [46, 47] and Chronic Kidney Disease (CKD) [32].

The present study investigates the suitability of SRPs by comparing them with RGs and examines trends of SRPs and RG in the MRB of Sri Lanka. The accuracy of SRPs is evaluated against RGs through continuous evaluation and categorical indices. In addition, the trend analysis of precipitation products was carried out using the Mann-Kendall test and Sen's slope methods. The current study is the first of

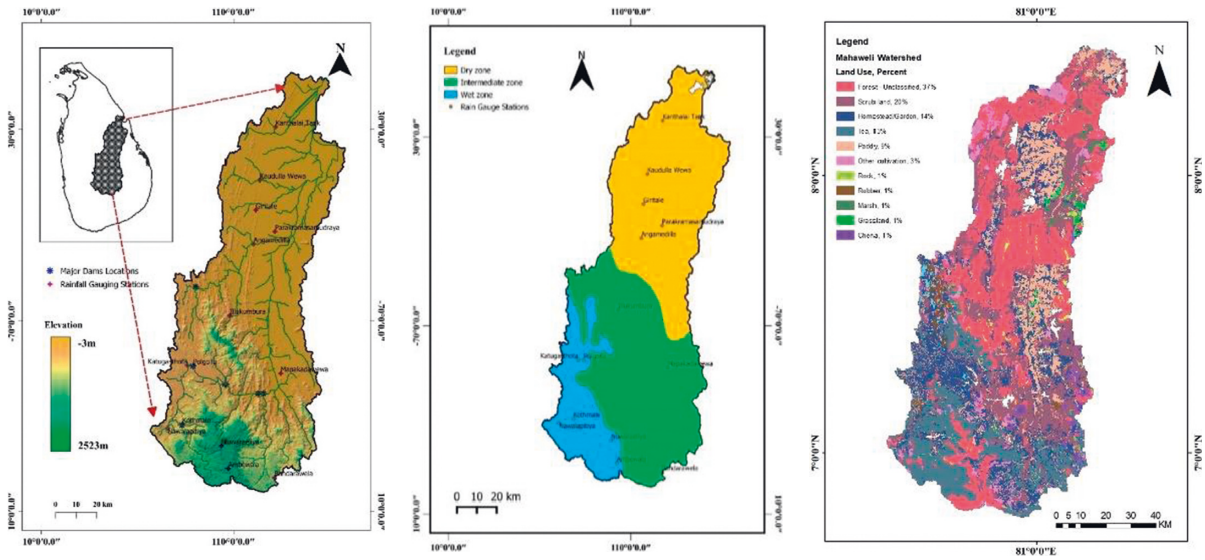

(a) (b) (c)

Figure 1: Maps of MRB, Sri Lanka. (a) The Mahaweli River Basin, Sri Lanka. (b) Climate zones of the MRB. (c) Land use map of the MRB.

its kind which examines the efficiency of SRPs over the MRB. Hence, the present study carries a significant novelty to the research community, opening doors for the use of SRPs in the absence of RG data in the MRB. Stakeholders of the MRB including river basin authorities, agriculturists, meteorologists, hydrologists, and stakeholders (including government authorities and farmers) will be benefited from the results of the study.

2. Study Area and Datasets

2.1. Study Area. The MRB is the longest river in Sri Lanka extending to 335 km. The Mahaweli River starts from the SriPada Mountains in the central hills. The drainage area of the MRB is 10,448 km^2, covering one-sixth of the landmass in the country. Figure 1(a) illustrates the elevation map of MRB obtained by extracting Digital Elevation Models (DEMs) from the Shuttle Radar Topography Mission (SRTM) with a resolution of 30 m × 30 m. Depending on the climatic and geographical distribution of annual rainfall amount, three climatic regions (wet, intermediate, and dry zones) fall in the MRB (Figure 1(b)) [36].

The annual rainfall in the country is influenced by four monsoon seasons of Southwest Monsoon (SWM) from May to September, Northeast Monsoon (NEM) from December to February, first intermonsoon (FIM) during March and April, and second intermonsoon (SIM) during October and November. Having the wet zone of the river basin in the southwest part of the country and the dry zone in the northeast part, the annual rainfall on the MRB is dependent on all these four seasons with the main ones being SWM and NEM [48]. The river basin in three climatic zones can be clearly seen in Figure 2(a). The annual rainfall in this basin is estimated to be 2500 mm of which 900 mm is discharged back to the sea. This produces an annual average discharge of 8.4 billion m^3 in the basin [49]. Tea estates and forest areas can abundantly be seen upstream of the MRB, whereas cultivated areas are frequent downstream of MRB. The land-use types of MRB obtained from the Department of Surveys, Sri Lanka, with a resolution of 1 km × 1 km are given in Figure 1(c). Therefore, as illustrated in Figure 1(c), the upper catchment of the MRB is mainly occupied by agricultural lands (mostly tea cultivation) while the lower catchment is by forest cover.

2.2. Datasets

2.2.1. Rain Gauge Data. For the analysis of this study, based on the availability of rainfall data, 14 rain gauge stations in the wet, the intermediate, and the dry zones of the MRB were obtained from the Department of Meteorology, Sri Lanka. The selected 14 rain gauge stations with their location and period are listed in Table 1. The missing data percentage in the rain gauge stations was below 5%; therefore, rainfall data from neighboring stations were used to fill the missing values. The average rain gauge density in the Mahaweli catchment is 1.34 gauges per 1000 km^2. This is a significantly high value when compared with several other studies. Mu et al. [50] had an average rain gauge density of 0.53 gauges per 1000 km^2, Paca et al. [51] had 0.11 gauges per 1000 km^2, and Calvante et al. [52] had only 0.01 gauges per 1000 km^2.

2.2.2. Satellite Rainfall Products. Similar to the gauge measurements, satellite rainfall products were also obtained for the 14 station locations mentioned in Table 1. Six SRPs (Table 2) used in this analysis are Precipitation Estimation from Remotely Sensed Information using Artificial Neural Networks (PERSIANN), Precipitation Estimation from Remotely Sensed Information using Artificial Neural Networks–Cloud Classification System (PERSIANN-CCS), Precipitation Estimation from Remotely Sensed Information

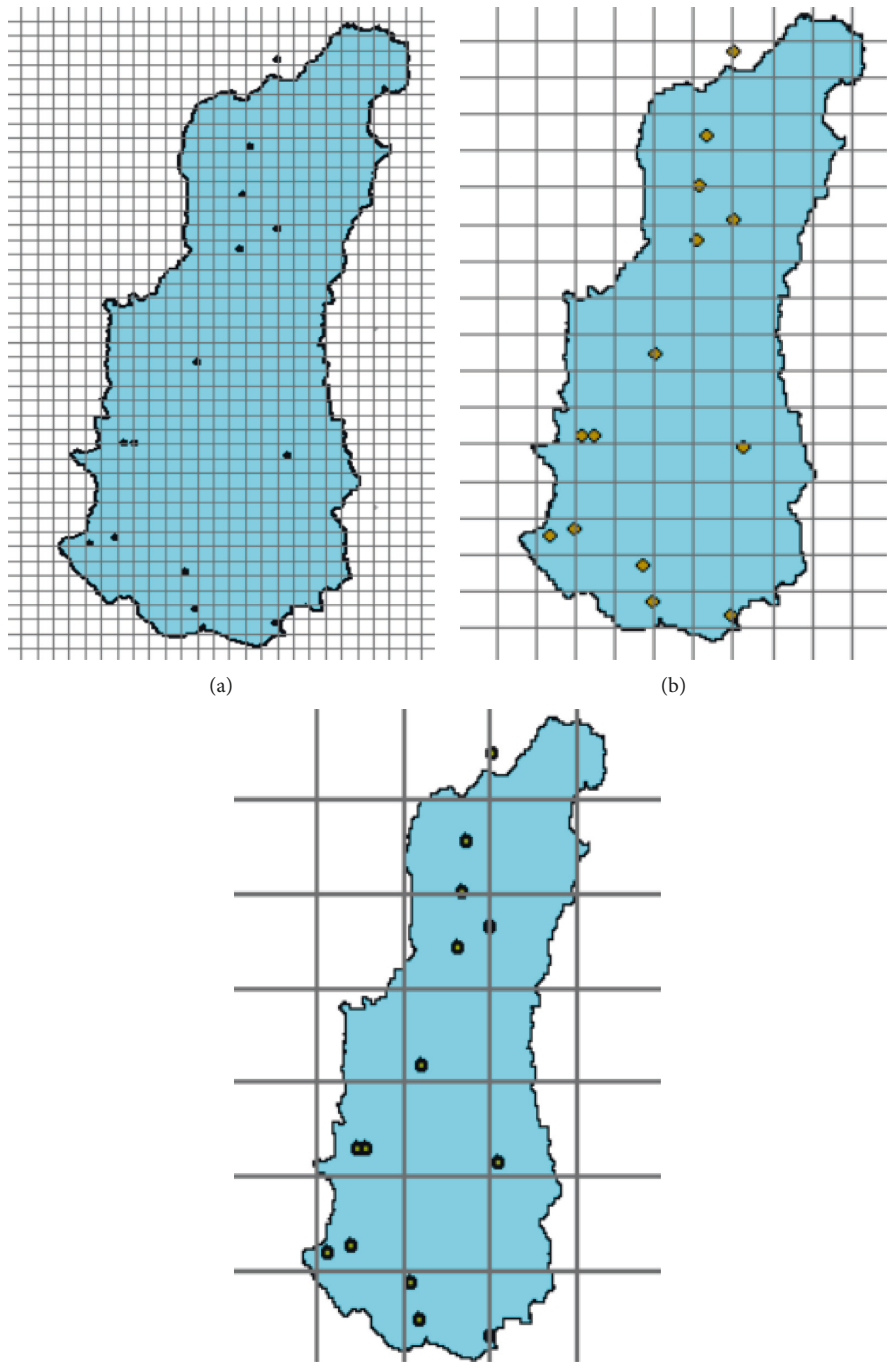

Figure 2: Grid layout and location of RGs. (a) For $0.04^{\circ} \times 0.04^{\circ}$. (b) For $0.10^{\circ} \times 0.10^{\circ}$. (c) For $0.25^{\circ} \times 0.25^{\circ}$.

using Artificial Neural Networks–Climate Data Record (PERSIANN-CDR), Integrated MultisatellitE Retrievals for GPM (IMERG) Version 6, Tropical Rainfall Measuring Mission (TRMM) Multisatellite Precipitation Analysis (TMPA) 3B42 (Version 7), Tropical Rainfall Measuring Mission (TRMM) Multisatellite Precipitation Analysis (TMPA) 3B42RT (Version 7), and Integrated MultisatellitE Retrievals for Global Precipitation Measurements (IMERG). The grid layout and location of RGs are demonstrated in Figure 3.

TRMM-3B42 and 3B42RT: TRMM 3B42/3B42RT satellite products were produced through a combined mission between the National Aeronautics and Space Association (NASA) and the Japan Aerospace Exploration Agency (JAXA) with the finest temporal resolution of 3 hours and a spatial resolution of $0.25^{\circ} \times 0.25^{\circ}$. TRMM 3B42 version 7 product is a research-grade satellite product and is one out of the two products of TRMM 3B42 retrievals. TRMM Combined Instrument (TCI) estimate employing TRMM Microwave Imager (TMI) and the Precipitation Radar (PR)

Table 1: Details of rain gauge stations.

Rain gauge stations	Latitude	Longitude	Timespan
Ambewala	6° 52′ 9.36″N	80° 47′ 44.34″E	1983–2016
Angamedilla	7° 51′ 18″N	80° 54′ 25.19″E	1983–2018
Bandarawela	6° 49′ 47.88″N	80° 59′ 52.71″E	1983–2016
Giritale	8° 0′ 16.10″N	80° 54′ 58.58″E	1983–2017
Illukumbura	7° 32′ 38.86″N	80° 48′ 6.43″E	1983–2015
Kanthalai tank	8° 22′ 16.47″N	81° 0′ 10.46″E	1987–2018
Katugasthota	7° 19′ 26.78″N	80° 37′ 13.96″E	1990–2019
Kaudulla wewa	8° 8′ 12.52″N	80° 56′ 1.86″E	1983–2017
Kothmale	7° 3′ 52.91″N	80° 35′ 54.79″E	1985–2018
Mapakadawewa	7° 17′ 21.55″N	81° 1′ 32.78″E	1983–2016
Nawalapitiya	7° 2′ 51″N	80° 32′ 3.99″E	1989–2017
Nuwaraeliya	6° 58′ 11.99″N	80° 46′ 11.99″E	1990–2019
Parakramasamudraya	7° 54′ 36.23″N	81° 0′ 1.78″E	1983–2018
Polgolla	7° 19′ 20.98″N	80° 38′ 45.94″E	1988–2018

Table 2: Details of SRPs used in the study.

Product	Data provider	Temporal coverage	Finest time resolution	Spatial resolution	Spatial coverage
TRMM-3B42 V7	NASA[1]	01/1998 to 12/2019	3 hours	0.25° × 0.25°	50°N-50°S
TRMM-3B42RT V7	NASA	03/2000 to 12/2019	3 hours	0.25° × 0.25°	60°N-560°S
IMERG V06	NASA	06/2000 to present	30 minutes	0.10° × 0.10°	90°N-90°S
PERSIANN	CHRS[1]	03/2000 to present	1 hour	0.25° × 0.25°	60°N-60°S
PERSIANN-CSS	CHRS	01/2003 to present	1 hour	0.04° × 0.04°	60°N-60°S
PERSIANN-CDR	CHRS	01/1983 to present	1 day	0.25° × 0.25°	60°N-60°S

[1] Center for Hydrometeorology and Remote Sensing (CHRS).
[2] National Aeronautics and Space Administration, USA (NASA).

data are the sources used to estimate precipitation through the TRMM satellite [12]. The spatial coverage of TRMM is between 50°N and 50°S [53]. This rainfall data is produced after two months from the observation time and is called a post-real-time product. The combined use of microwaves, infrared waves, and ground observed rainfall measurements makes it a better product in estimating rainfalls overall [19]. TRMM 3B42RT version 7 is a near-real-time product which is the remaining product of TRMM 3B42 retrievals.

IMERG: Integrated MultisatellitE Retrievals for Global Precipitation Measurements (IMERG) is another satellite product developed by NASA. The recently released version (V06 B) of IMERG Final Run was used in this study. This product has a spatial resolution of 0.10° × 0.10° and spatial coverage of 50°N-50°S. Moreover, the finest temporal resolution is 30 minutes. IMERG product is based on low-earth orbit satellites and geostationary satellites together with high spatiotemporal observed rainfall data. The algorithm used to produce IMERG is intended to intercalibrate, merge, and interpolate "all" satellite microwave precipitation estimates, together with microwave-calibrated infrared satellite estimates, precipitation gauge analyses, and potentially other precipitation estimators. The V06B product is considered a huge improvement over the superseded versions of IMERG since it was updated further in data processing, algorithms, and verification which effectively enhanced its detection accuracy [54, 55].

PERSIANN: Artificial Neural Network (ANN) algorithm is used in Precipitation Estimation from Remotely Sensed Information using Artificial Neural Networks (PERSIANN) to estimate rainfall. In order to estimate precipitation through PERSIANN IR brightness temperature data from global geostationary satellites is obtained from Climate Prediction Center (CPC) and National Oceanic and Atmospheric Administration (NOAA). This product is available from 2000 to the present and the finest temporal coverage of 1 hour is available. The spatial resolution of the product is 0.25° with a spatial coverage of 60°N-60°S. In order to account for the high uncertainties in associating the relationships between precipitation and cloud-top brightness temperature due to cloud properties and atmospheric conditions, the ANN parameters are updated with rainfall estimates from low-orbital satellites whenever independent estimates of rainfall are available [14, 56].

PERSIANN-CCS: PERSIANN-Cloud Classification System (PERSIANN-CCS) is a real-time global high-resolution SRP. The ANN algorithm used in PERSIANN-CCS extracts local and regional cloud features from infrared geostationary satellite imagery. The information is extracted from the whole cloud patch and provides multiple infrared brightness temperature versus rainfall rate relationships for different cloud classification types enabling this product to generate variable rain rates at a given brightness temperature and variable rain/no-rain IR thresholds for different cloud types

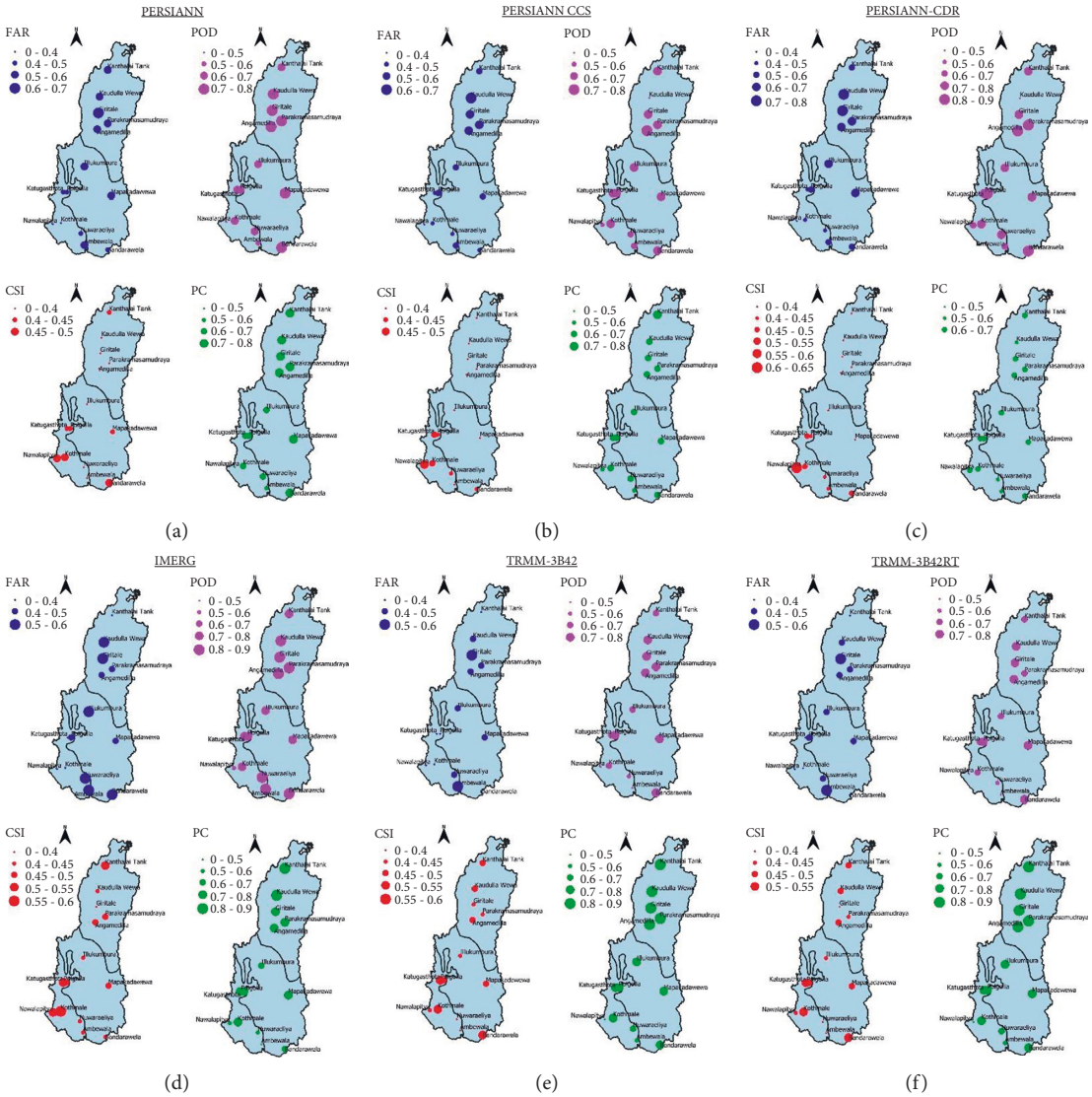

Figure 3: Categorical evaluation for light rainfall events. (a) For PERSIANN. (b) For PERSIANN-CCS. (c) For PERSIANN-CDR. (d) For IMERG. (e) For TRMM-3B42. (f) For TRMM-3B42RT.

[57, 58]. This product has a spatial resolution of $0.04^\circ \times 0.04^\circ$ and the finest temporal frequency of 1 hour is available. The PERSIANN-CCS data is available from 2003 to the present.

PERSIANN-CDR: PERSIANN-Climate Data Record (PERSIANN-CDR) developed using the PERSIANN algorithm was developed from the National Climatic Data (NCDC) CDR program of the National Oceanic and Atmospheric Administration (NOAA) [59]. The finest temporal resolution of this product is 1 day with a 60°N-60°S spatial coverage and a $0.25^\circ \times 0.25^\circ$ spatial resolution. Infrared brightness temperature CDR from Gridded Satellite (GridSat)-B1 of the International Satellite Cloud Climatology Project (ISCCP) is used as the input used to train the neural network of the PERSIANN model [19]. The PERSIANN-CDR data obtained were then bias-corrected using 2.5° monthly Global Precipitation Climatology Project (GPCP) data. This SRP was mainly developed with the aim of providing a long-term, high-resolution, and global precipitation dataset to be used in studies to determine changes and trends in daily precipitation, especially extreme precipitation events, due to climate change and natural variability [60].

2.2.3. Data Extraction. The six satellite products used in this study were extracted in different methods. PERSIANN group of products were directly obtained from the CHRS data portal as CSV files. IMERG and TRMM products were obtained as NetCDF (Network Common Data Form) files from the NASA GESDISC portal. Afterward, IMERG was extracted through the process of merging the files in Climate Data Operator (CDO) followed by the extraction using *R* coding in RStudio. The TRMM products were merged using a similar approach as in IMERG, but the extraction of the point rainfall data was done using MATLAB 9.6.

2.3. Overall Methodology. Statistical indices were used to determine the accuracy of the satellite data sets with respect

to RG data. Nonparametric tests were used to analyze the trend and to find the magnitude of the trends observed.

2.3.1. Categorical Evaluation Indices. To examine the detection accuracy of SRPs, there are four categorical indices, namely, the False Alarm Ratio (FAR), the Critical Success Index (CSI), the Probability of Detection (POD), and the Proportion Correct (PC). FAR gives the fraction of times the satellite detects rainfall events that did not actually occur. POD provides a quantitative measure of the number of times the satellite will detect rainfall events accurately. CSI provides the fraction of times the rain gauge and/or SRP data were correctly predicted and PC provides a quantitative measure of the accuracy of the detected rainfall [61]. The equations (1)–(4) associated with each of the indices are as given below.

False Alarm Ratio (FAR)

$$\mathbf{FAR} = \frac{\mathbf{T_F}}{\mathbf{T_H} + \mathbf{T_F}}. \quad (1)$$

Probability of Detection (POD)

$$\mathbf{POD} = \frac{\mathbf{T_H}}{\mathbf{T_H} + \mathbf{T_M}}. \quad (2)$$

Critical Success Index (CSI)

$$\mathbf{CSI} = \frac{\mathbf{T_H}}{\mathbf{T_H} + \mathbf{T_M} + \mathbf{T_F}}. \quad (3)$$

Proportion Correct (PC)

$$\mathbf{PC} = \frac{\mathbf{T_H} + \mathbf{T_C}}{\mathbf{T_H} + \mathbf{T_M} + \mathbf{T_F} + \mathbf{T_C}}, \quad (4)$$

where H represents the rainfall accurately detected (correct hits), **M** represents the rainfall not detected (missed data), **F** represents the precipitation that was falsely detected (false alarms), **C** represents the correct negatives, and $\mathbf{T_F}$, $\mathbf{T_H}$, $\mathbf{T_M}$, and $\mathbf{T_F}$ are the number of times each of the cases occurred, respectively.

The analysis using categorical indices was done for 1 mm/day and 10 mm/day thresholds representing light and heavy rainfall, respectively. The threshold to represent light and heavy rainfall was decided based on Table 3 [62] and the contingency table used for the analysis is shown in Table 4.

If the rainfall threshold = x mm, the categorical indices were calculated based on the following conditions.

2.3.2. Continuous Evaluation Indices. Continuous evaluation indices were used to evaluate the performance of SRP with respect to RG data. To find out the extent to which these two datasets agree with each other (correlation), Pearson's correlation coefficient (CC) was used. To determine the absolute average magnitude of the error between the two datasets, Mean Absolute Error (MAE) was used. Root Mean Square Error (RMSE) which gives more relevance to the larger errors when compared with MAE was used again to determine the absolute average error magnitude. To determine the degree of overall underestimation or overestimation, Relative Bias (RB) was used [61, 64, 65]. Finally, to measure the goodness of fit between the observed and SREs which was initially developed by Gupta et al. [66] and further modified by Kling et al. [67], Kling Gupta Efficiency (KGE) was used. KGE is less sensitive to extreme rainfall and therefore can interpret the overall fitness of rainfall having different intensities [68]. Equations (5)–(9) associated with each of the indices are as given below.

Table 3: Rainfall intensities and thresholds.

Intensity class of rainfall	Rainfall thresholds per day
No/tiny rainfall	$P < 1$ mm
Light rainfall	1 mm $\le P <$ 2 mm
Low moderate rainfall	2 mm $\le P <$ 5 mm
High moderate rainfall	5 mm $\le P <$ 10 mm
Heavy rainfall	$P \ge 10$ mm

Table 4: Contingency table for categorical indices [63].

Satellite events (x in mm)	Observation event (x in mm)	
	Yes ($P \ge x$)	No ($P < x$)
Yes ($P \ge x$)	Hits	False alarms
No ($P < x$)	Misses	Correct negatives

Pearson's correlation coefficient (CC)

$$\mathbf{CC} = \frac{\sum_{\mathbf{i}=1}^{\mathbf{n}} (\mathbf{G_i} - \overline{G})(\mathbf{S_i} - \overline{\mathbf{S}})}{\sqrt{\sum_{\mathbf{i}=1}^{\mathbf{n}} (\mathbf{G_i} - \overline{\mathbf{G}})^2 \mathbf{x} \sqrt{\sum_{i=1}^{n} (\mathbf{S_i} - \overline{\mathbf{S}})^2}}}. \quad (5)$$

Mean Absolute Error (MAE)

$$\mathbf{MAE} = \frac{1}{\mathbf{n}} \sum_{\mathbf{i}=1}^{\mathbf{n}} |\mathbf{S_i} - \mathbf{G_i}|. \quad (6)$$

Root Mean Square Error (RMSE)

$$\mathbf{RMSE} = \sqrt{\frac{1}{\mathbf{n}} \sum_{\mathbf{i}=1}^{\mathbf{n}} (\mathbf{S_i} - \mathbf{G_i})^2}. \quad (7)$$

Relative Bias (RB)

$$\mathbf{RB} = \frac{(1/\mathbf{n}) \sum_{\mathbf{i}=1}^{\mathbf{n}} (\mathbf{S_i} - \mathbf{G_i})}{\overline{\overline{\mathbf{G}}}} \times 100\%. \quad (8)$$

Kling Gupta Efficiency.

$$\mathbf{KGE} = 1 - \sqrt{(\mathbf{CC} - 1)^2 + \left(\frac{\mathbf{S_d}}{\mathbf{G_d}}\right)^2 + \left(\frac{\overline{\mathbf{S}}}{\overline{\overline{\mathbf{G}}}}\right)^2}, \quad (9)$$

where $\mathbf{S_i}$, $\overline{\mathbf{S}}$, and $\mathbf{S_d}$ (*for SRP data*) are the $\mathbf{i^{th}}$ station, mean values of SRP data, and standard deviation of SRP data, respectively, $\mathbf{G_i}$, $\overline{\mathbf{G}}$, and $\mathbf{G_d}$ (*for Rain gauge data*) are the $\mathbf{i^{th}}$ station, mean values of gauge data, and standard deviation of gauge data, respectively, and **n** represents the total number of data considered.

The strength range of correlation coefficient (CC) was defined as interpreted by The Political Sciences Department at Quinnipiac University [69] and is given in Table 5.

Table 5: Correlation coefficient interpretation.

Correlation coefficient		Interpretation
+1	−1	Perfect
+0.9 to +0.7	−0.9 to −0.7	Very strong
+0.6 to +0.4	−0.6 to −0.4	Strong
+0.3	−0.3	Moderate
+0.2	−0.2	Weak
+0.1	−0.1	Negligible
0	0	None

2.3.3. Nonparametric Tests. To analyze the presence of trends in the RG and SRP data, the Mann-Kendall (MK) test was used. The Theil's & Sens Slope Estimator was used to quantify the trends.

Mann-Kendall (MK) Test. The MK test [70, 71] provides the significance of the trends that are observed in the rain gauge and satellite data. MK Test uses the hypothesis of H_0 for no trend scenario and H_1 when a trend is present in the datasets. The Mann-Kendall Statistic S is given by the following equation:

$$\mathbf{S} = \sum_{\mathbf{i}=1}^{\mathbf{n}-1} \sum_{\mathbf{j}=\mathbf{i}+1}^{\mathbf{n}} \operatorname{sgn}\left(\mathbf{x_j} - \mathbf{x_i}\right), \tag{10}$$

$$\text{where } \operatorname{sgn}(\mathbf{x_j} - \mathbf{x_i}) = \begin{cases} +1 & > (\mathbf{x_j} - \mathbf{x_i}) \\ 0 & = (\mathbf{x_j} - \mathbf{x_i}) \\ -1 & < (\mathbf{x_j} - \mathbf{x_i}) \end{cases}.$$

An increasing trend will be the outcome if S is having a very high positive value and decreasing trend if S is having a very low negative value. To compute the probability associated with the calculated S and the sample size to obtain a significance of the trend, [71] describes a normal approximation test incorporating the Mann-Kendall Statistic, S. A normalized test statistic Z is computed along with the probability associated with the Z value, $f_{(z)}$.

$$\mathbf{Z_c} = \begin{cases} \dfrac{\mathbf{S} - 1}{\sqrt{\mathbf{Var}(\mathbf{S})}}, & \mathbf{S} > 0, \\ 0, & \mathbf{S} = 0, \\ \dfrac{\mathbf{S} + 1}{\sqrt{\mathbf{Var}(\mathbf{S})}}, & \mathbf{S} < 0, \end{cases} \tag{11}$$

where
$\mathbf{Var}(\mathbf{S}) = (\mathbf{n}(\mathbf{n}-1)(2\mathbf{n}+5) - \sum_{\mathbf{i}=1}^{\mathbf{t}} \mathbf{t}_i(\mathbf{i})(\mathbf{i}-1)(2\mathbf{i}+5))/18$,
where $\mathbf{n}$ is the number of datasets, $\mathbf{t}$ is the number of tied groups, and $\mathbf{t_i}$ is the number of datasets in the $\mathbf{i^{th}}$ group.

The probability density function $f_{(z)}$ for a normal distribution with a mean of 0 and a standard deviation of 1 is given by

$$f(z) = \frac{1}{\sqrt{2\pi}} \mathbf{e}^{\mathbf{z}^2/2}. \tag{12}$$

Taking a 95% significance level, the trend will be determined to be decreasing if Z is negative and the probability is greater than 0.95. Similarly, the trend will be determined to be increasing if Z is positive and the probability is greater than 0.95. If the probability is lesser than 0.95, then it was concluded that no trend is present in the datasets [72].

Theil-Sens Slope Estimator Test. To quantify and obtain a magnitude of the trends observed from the MK test, Sens Slope Estimator was used [73]. Since the data sets used correspond to the same time intervals and upon arranging the data sets in ascending order with time, the slope of each time series data pair was calculated using the following equation:

$$\mathbf{Q_k} = \frac{\mathbf{X_j} - \mathbf{X_k}}{\mathbf{j} - \mathbf{i}}, \tag{13}$$

where $j > k$, X corresponds to a data value at a j/k time and $k = 1, 2, \ldots N$

Upon arranging the $\mathbf{N}$ values in ascending order, the median value of the Sens Slope $\mathbf{Q_i}$ will be calculated using the equation given below:

$$\mathbf{Q_i} = \begin{cases} \mathbf{Q}_{(\mathbf{n}+1)/2}, & \textbf{if N is odd}, \\ \dfrac{1}{2}\left(\mathbf{Q}_{\mathbf{n}/2} + \mathbf{Q}_{\mathbf{n}+2/2}\right), & \textbf{if N is even}. \end{cases} \tag{14}$$

3. Results and Discussion

3.1. Detection of Light Rainfall Events. The mean values calculated for each satellite product after the calculation of categorical indices with the 14 rainfall gauge stations yielded the following results. Figure 4 shows the graphical representation of the obtained results. The threshold used for the light rainfall representation was 1 mm/day. The best performance in terms of FAR was shown by TRMM-3B42 and TRMM-3B42RT products with a mean value of 0.40 and a stationwise variation of 0.01 to 0.54 while the worst performance was shown by PERSIANN-CDR with a mean of 0.54 and a stationwise variation of 0.01 and 0.75. With respect to POD and CSI, the best performance was shown by the IMERG rainfall with a mean of 0.79 and 0.47, respectively, as further proved by Moazami et al. [74]. Stationwise distribution of these indices was 0.47 to 0.88 in POD and 0.37 to 0.57 in CSI. The worst performance in POD was represented by TRMM-3B42 with a mean of 0.66, and in CSI, PERSIANN-CCS and CDR showed the worst performances giving a mean of 0.39. TRMM-3B42 performed best in PC with a mean of 0.73 and stationwise variation of 0.41 to 0.84 while PERSIANN-CDR showed the worst performance with a mean value of 0.62 and stationwise variation of 0.55 and 0.68. From the stationwise mean values, IMERG turned out to be the best, having high performances in both the number of times of accurate rainfall detection (POD) and correct rainfall prediction (CSI). PERSIANN-CDR proved to be the worst by performing the worst rainfall detection (PC), the number of times of correct rainfall prediction (CSI), and the highest fraction of false rainfall ratio (FAR). When comparing the categorical indices results with the climatic zone distribution of stations, IMERG stood out in

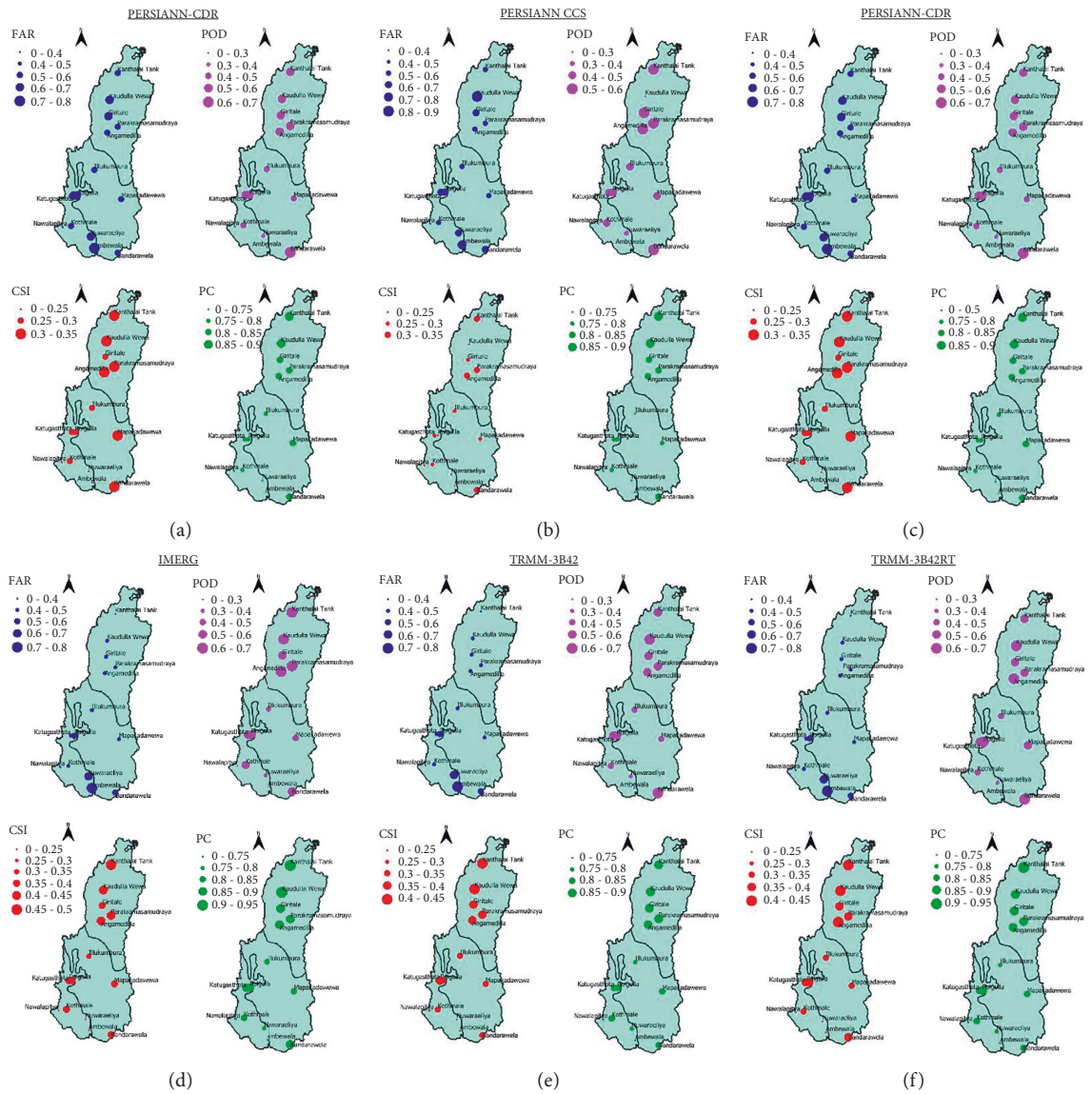

Figure 4: Categorical evaluation for heavy rainfall events. (a) For PERSIANN. (b) For PERSIANN-CCS. (c) For PERSIANN-CDR. (d) For IMERG. (e) For TRMM-3B42. (f) For TRMM-3B42RT.

POD and CSI having higher mean values in both dry and wet zones. TRMM-3B42 also performed well in both FAR and PC in wet and dry zones, respectively. PERSIANN-CDR performed badly in dry zones in both FAR and PC and CSI in the wet zone.

3.2. Detection of Heavy Rainfall Events. The results for categorical indices for each satellite product with a 10 mm/day threshold to represent heavy rainfall are summarized below. Figure 5 shows the graphical representation of the obtained results.

Best performance in FAR, POD, and CSI was shown by IMERG product with a mean value of 0.47, 0.5, and 0.35, respectively, which were in consistent with the range of values obtained in a study done in China incorporating different IMERG products [75]. The stationwise variation was 0.05 to 0.79, 0.18 to 0.64, and 0.12 to 0.46, respectively. The worst performance in FAR was shown by PERSIANN-CCS with a mean of 0.62 and stationwise variation of 0.06 and 0.84. In both POD and CSI, the worst performances were shown by PERSAINN-CDR with a mean value of 0.41 and 0.24, respectively. TRMM-3B42 and 3B42-RT performed best in PC with a mean of 0.81 and stationwise variation of 0.25 and 0.9 while PERSIANN-CCS showed the worst performance with a mean value of 0.77 and stationwise variation of 0.27 and 0.86. From the stationwise mean values, IMERG turned out to be the best, having high performances in having a lower fraction of false rainfall ratio (FAR), the number of times of accurate rainfall detection (POD), and reasonably accurate rainfall prediction (CSI). PERSIANN-CDR proved to be the worst by performing poorly in both the number of times of accurate rainfall detection (POD) and correct rainfall prediction (CSI). Similarly, PERSIANN-

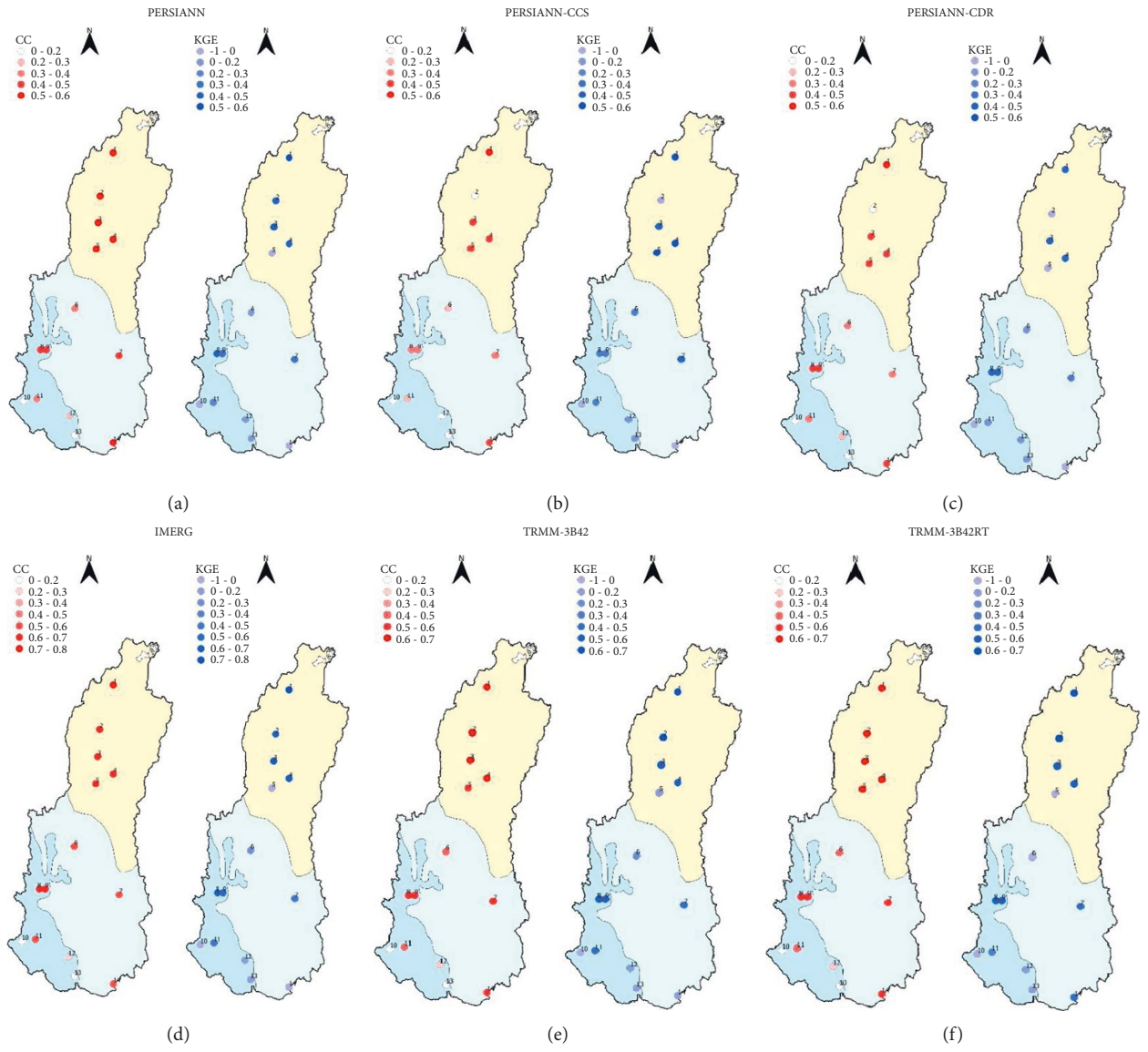

Figure 5: CC and KGE results for daily time scale. (a) For PERSIANN. (b) For PERSIANN-CCS. (c) For PERSIANN-CDR. (d) For IMERG. (e) For TRMM-3B42. (f) For TRMM-3B42RT.

CCS also proved to be the worst by performing relatively badly in both accurate rainfall detection (PC) and the number of times of correct rainfall prediction (CSI).

When comparing the climatic zone distribution of stations with the categorical indices, IMERG stood out in all four indices having higher mean values in dry zones. PERSIANN-CCS performed worst in both POD and CSI in wet zones and in FAR in dry zones. Likewise, PERSIANN-CDR also poorly performed in FAR and POD in dry and wet zones, respectively.

After comparing all the results obtained from light and heavy rainfall detection, it was clear that IMERG outstands the highest with a value of 0.9 in PC which is the highest out of all mean values recorded. It showed this higher accuracy mainly in the dry zones of the river basin. A study carried out on the performance evaluation of SRPs over varying climates and complex topographies has also proved this finding with the IMERG product [76]. PERSIANN-CCS and CDR were found to outstand the least having mean values in the range of 0 to 0.4 in both POD and CSI. This was further proved by Gadouali et al. [60], who performed a study on SRPs in Morocco. His results showed that PERSIANN-CDR was worst at detecting rainfalls. Another study which was performed on the evaluation and comparison of SRPs in Burkina Faso, West Africa, also proved the same with PERSIANN products [77].

3.3. Continuous Evaluation Indices. The correlation between the observed and satellite rainfall data was observed for both daily and monthly time scales. In both time scales, all CCs were in the range of $0 < CC < 1$, showing an overall positive correlation in all products. Out of the six satellite products, the highest median of 0.6 was observed in the IMERG

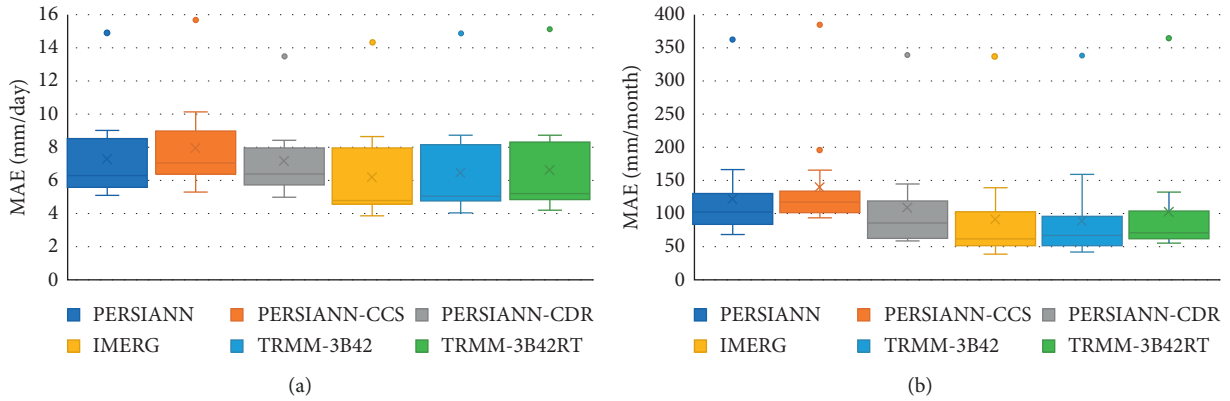

Figure 6: Results obtained from the MAE index. (a) For Daily. (b) For Monthly.

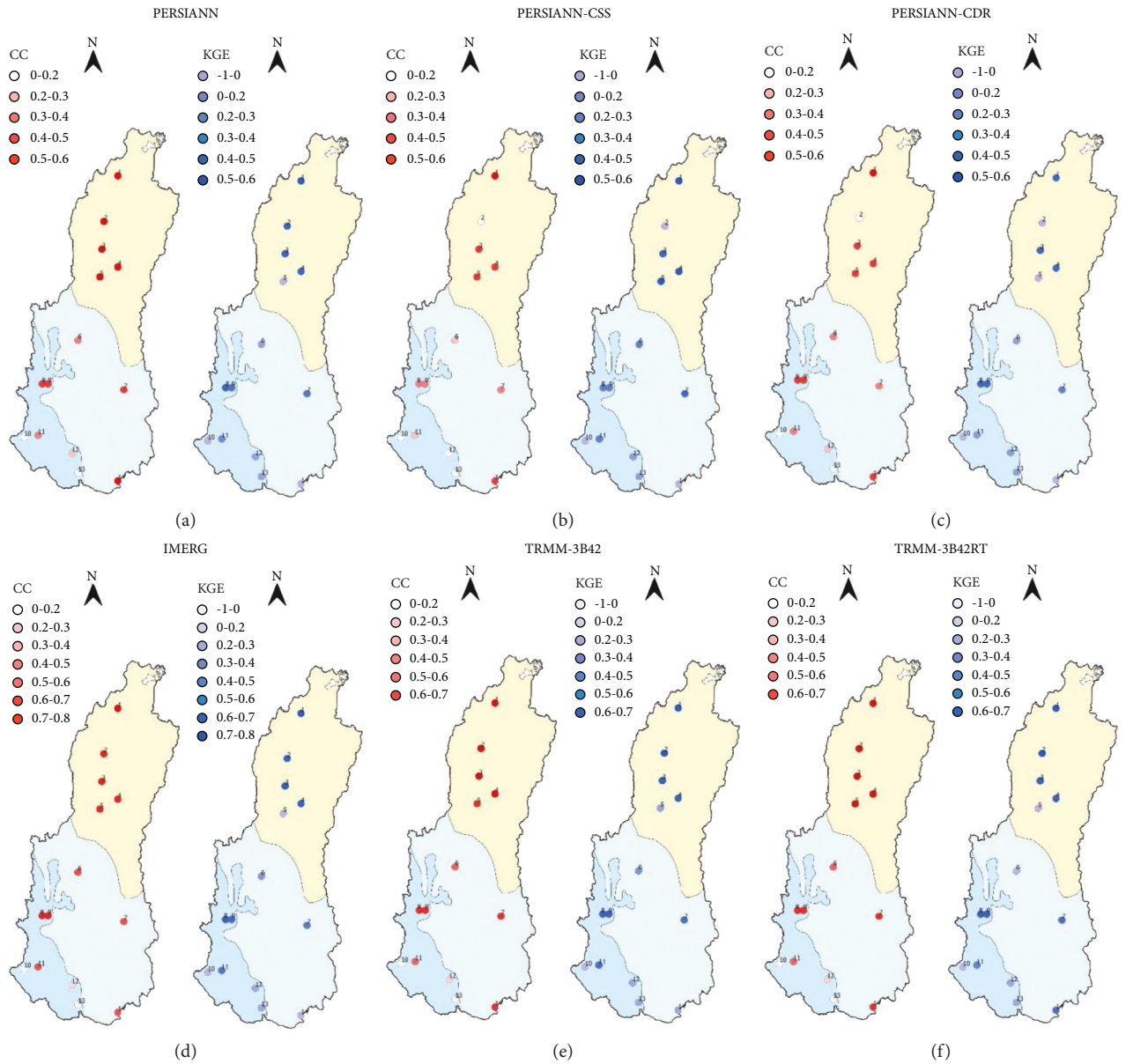

Figure 7: MK and Sen's Slope results for annual analysis. (a) For Observed rainfall data. (b) For PERSIANN. (c) For PERSIANN-CCS. (d) For PERSIANN-CDR. (e) For IMERG. (f) For TRMM-3B42. (g) For TRMM-3B42RT.

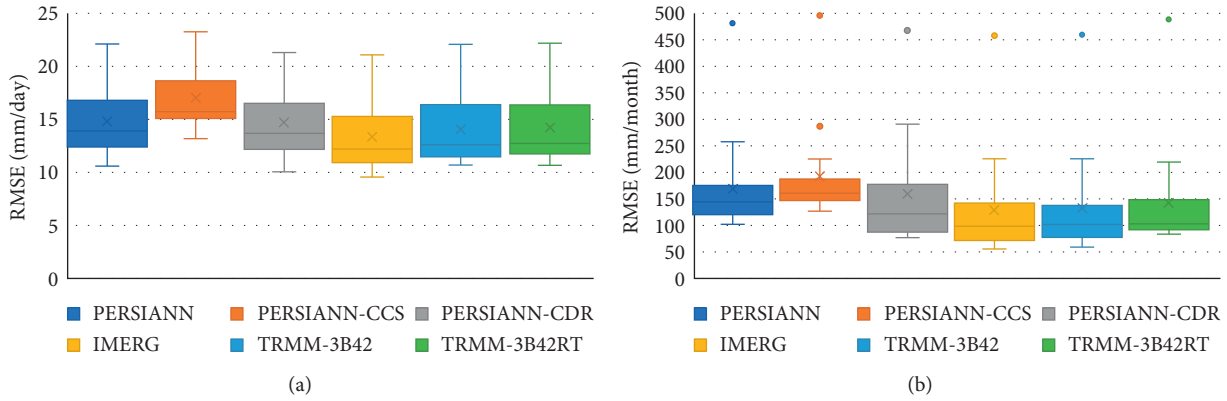

Figure 8: (a) For PERSIANN. (b) For PERSIANN-CCS. (c) For PERSIANN-CDR. (d) For IMERG. (e) For TRMM-3B42. (f) For TRMM-3B42RT.

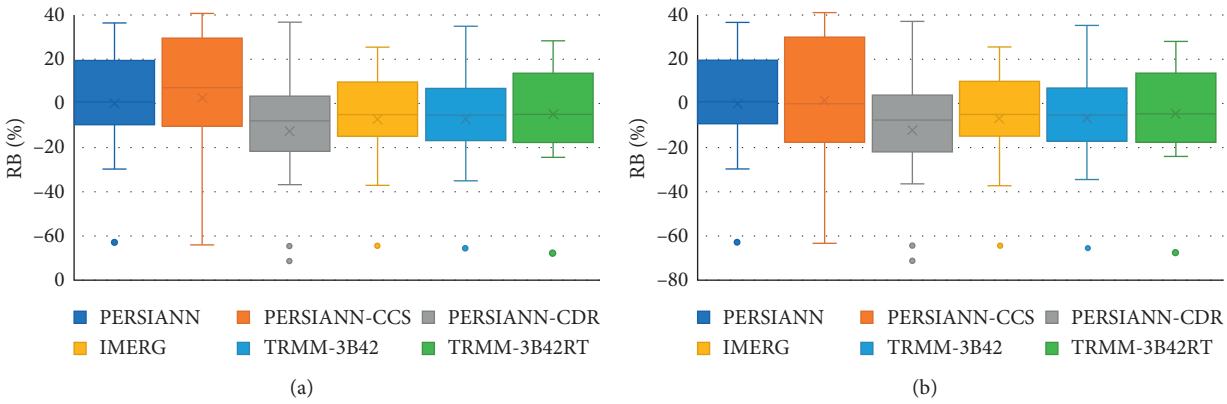

Figure 9: Results obtained from the RMSE index. (a) For Daily. (b) For Monthly.

product which interpreted a strong correlation. All the other products showed relatively poor correlation within the range of $0 < CC < 0.65$. In all 6 products, higher CC was observed mainly in dry zones while the lowest was identified in wet zones of the river basin. Studies conducted by Amjad et al. [76] in Turkey and Alijanian et al. [56] in Iran also showed that lower CC values are obtained for wet regions.

In the monthly time scale analysis, the highest median of 0.84 was shown by IMERG and TRMM-3B42 products. The highest positive values in both time scales were recorded from the dry zones of the river basin and the lower values from the wet zones. The order from strong positive to strong negative correlations was from IMERG and TRMM products to PERSIANN products in both time scales.

KGE shows a perfect fit when the value is close to 1 [68]. In both the daily and monthly analysis, IMERG showed the highest median value of 0.47 and 0.69 for daily and monthly scales, respectively. The worst fit of data was exhibited by PERSIANN-CDR on each time scale. All products showed relatively poor performance for daily data with all values less than 0.75. Most of the higher KGE values were observed in the dry zone and lower values were seen in the wet zones on the daily time scale. The goodness of fit within datasets was best with IMERG followed by TRMM products and PERSIANN products where the worst fit was observed. However, a better performance was observed by monthly values when compared with daily values.

Overall, both good correlation (CC) and fit between the datasets (KGE) were shown by the IMERG product further being proved by Adane et al. [78] from a similar study done in Northeastern Ethiopia. Poor correlation was mainly showcased by PERSIANN-CDR product. This poor performance can be a result of cloud-top IR observations as this product is mainly based on [15]. The graphical representation of the zonewise distribution of the results for the daily time scale from CC and KGE is shown in Figure 6 and the results of the same in monthly time scale are provided in Figure 7.

Both daily and monthly analyses with MAE, RMSE, and RB showed similar behavior (Figures 8–10, respectively). Out of the 6 products, the highest MAE was indicated by PERSIANN-CCS with a median of 7.09 mm/day and 110.01 mm/month in both daily and monthly analyses. On the other hand, IMERG turned out to have the lowest median MAE of 4.79 mm/day and 66.27 mm/month. The highest RMSE was reported by PERSIANN-CCS (median of 15.26 mm/day and 157.53 mm/month) and the lowest RMSE was from IMERG (median of 12.03 mm/day and 96.76 mm/month). All SRPs showed higher errors (MAE and RMSE) in

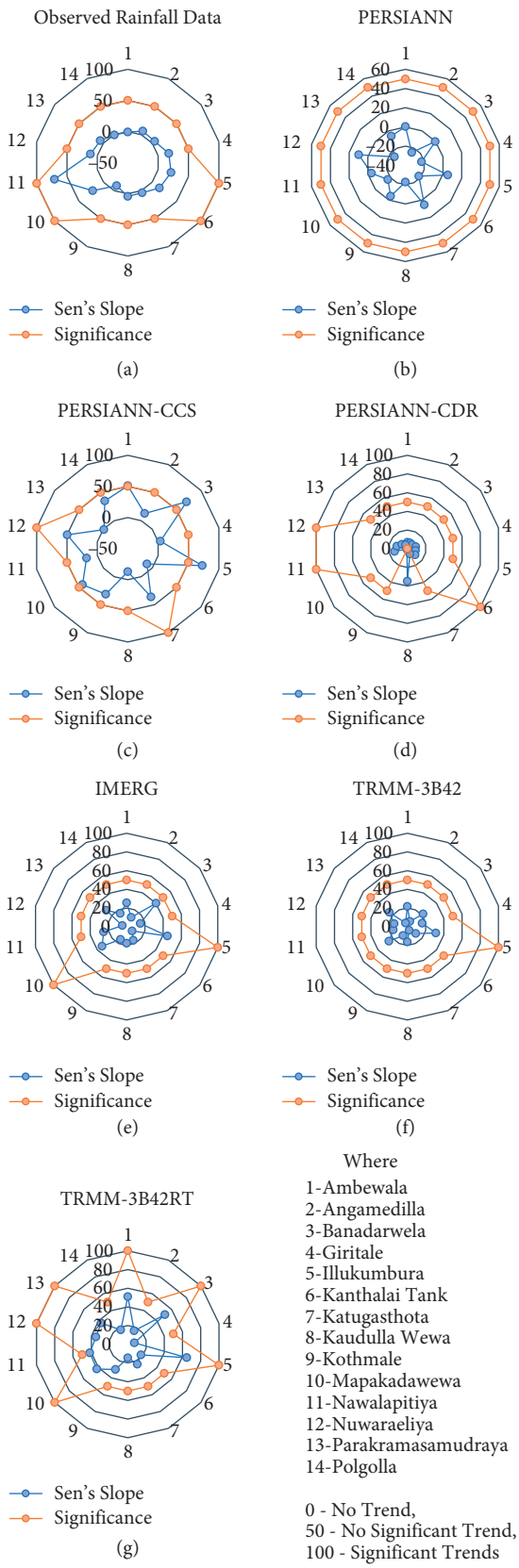

Figure 10: Results obtained from the RB index. (a) For Daily. (b) For Monthly.

the intermediate zone and lower errors in the dry zone of the river basin. This was further confirmed by a study done in Pakistan which stated that higher RMSE is prominent in regions having higher average annual rainfall [79]. The highest underestimation was shown by PERSIANN-CDR while the highest overestimation was from PERSIANN-CCS with medians of −7.55% and 7.79%, respectively. However, in monthly analysis, the highest underestimations were observed in PERSIANN-CDR and the highest overestimations were in PERSIANN product. All products showed higher underestimations in the intermediate zone and higher overestimations in the dry zone of the basin in both analyses.

Overall, it was noted that all SRPs are better at capturing rainfalls accurately with very less errors in the dry zone of the basin while the errors increased when moving from wet to the intermediate zone. IMERG was the best with very less errors in capturing accurate rainfalls when intercompared with the RG data. However, IMERG causes underestimations of rainfall data (median RB of −4.83% in both daily and monthly time scales). Comparatively, given that the IMERG product is set aside, TRMM products also showed better performance and PERSIANN products showed relatively the worst performances in all indices. The better performances of IMERG and TRMM products were further proved by Anjum et al. [80], who found that these products perform well with reference to the RG data at a monthly time scale. Also, overestimations were prominent only in PERISANN products while all other products produced underestimations.

From the performance shown in all the continuous evaluation indices, all products cannot efficiently reproduce the temporal variability in the observed rainfall gauge data on both daily and monthly time scales. Among the six evaluated products, IMERG followed by TRMM products performed well and PERSIANN products performed the worst in each index. Yang et al. [81] had yielded results similar to the present study. Their findings also showed that IMERG V06 and TRMM-3B42 V07 were in the best overall agreement with RG data in all temporal scales. Likewise, the categorical evaluation of these products is similar to what was observed from continuous evaluation indices. IMERG stood out here as well. The final run IMERG product, which is the product used in this study, has proved its higher performance in the Middle East as well [82]. It was also clear that these products possess significant errors which cannot be ignored when using them in hydrological applications. An approach for error correction would be required beforehand. Figures 8–10 show the box plot representation of the results for MAE, RMSE, and RB in both daily and monthly analyses, respectively.

3.4. Trend Analysis. Mann-Kendall trend test was used to identify any significant trends in the observed data and SRPs. Then, to quantify the trends obtained, Sen's slope estimator was used on the datasets.

Table 6: Monthly analysis of MK test and Sen's slope estimator significant trend results.

Observed data					
Station	Month	Kendall's Tau	*P* value (two-tailed)	Sen's slope (mm/month)	Remark
Ambewala	August	0.305	0.011	5.747	Significant Trend
Bandarawela	April	0.244	0.042	3.842	Significant Trend
Giritale	February	0.254	0.036	2.067	Significant Trend
	December	0.257	0.033	8.471	Significant Trend
Kanthalai Tank	September	−0.321	0.010	−3.873	Significant Trend
Katugasthota	July	−0.255	0.048	−2.273	Significant Trend
Mapakadawewa	April	0.239	0.047	3.213	Significant Trend
	May	0.270	0.025	1.896	Significant Trend
Nawalapitiya	April	0.265	0.048	4.008	Significant Trend
	December	0.379	0.004	7.584	Significant Trend
Nuwaraeliya	March	0.347	0.007	2.732	Significant Trend
	November	0.265	0.040	4.300	Significant Trend
Polgolla	July	−0.290	0.022	−2.088	Significant Trend
PERSIANN					
Station	Month	Kendall's Tau	*P* value (two-tailed)	Sen's slope (mm/month)	Remark
Kanthalai Tank	April	−0.427	0.011	−10.628	Significant Trend
Polgolla	May	0.357	0.033	12.650	Significant Trend
PERSIANN-CCS					
Station	Month	Kendall's Tau	*P* value (two-tailed)	Sen's slope (mm/month)	Remark
Ambewala	October	0.452	0.032	21.659	Significant Trend
Bandarawela	October	0.487	0.020	29.042	Significant Trend
	December	0.487	0.020	12.667	Significant Trend
Kanthalai Tank	April	−0.400	0.031	−14.964	Significant Trend
Katugasthota	August	0.353	0.048	13.143	Significant Trend
Kothmale	February	0.477	0.010	5.667	Significant Trend
	May	0.500	0.007	21.639	Significant Trend
Nawalapitiya	May	0.498	0.010	21.667	Significant Trend
Nuwaraeliya	May	0.353	0.048	16.500	Significant Trend
Parakramasamudraya	April	−0.377	0.043	−12.300	Significant Trend
Polgolla	May	0.494	0.008	20.545	Significant Trend
PERSIANN-CDR					
Station	Month	Kendall's Tau	*P* value (two-tailed)	Sen's slope (mm/month)	Remark
Ambewala	November	0.303	0.013	3.576	Significant Trend
	December	0.277	0.024	3.456	Significant Trend
Angamedilla	June	−0.301	0.011	−1.516	Significant Trend
	September	−0.324	0.006	−2.439	Significant Trend
	November	0.261	0.028	3.659	Significant Trend
Bandarawela	September	−0.248	0.039	−2.827	Significant Trend
	November	0.303	0.013	3.576	Significant Trend
	December	0.280	0.022	3.495	Significant Trend
Giritale	June	−0.241	0.045	−1.002	Significant Trend
	September	−0.298	0.013	−2.417	Significant Trend
	December	0.291	0.016	5.288	Significant Trend
Illukumbura	June	−0.337	0.006	−2.375	Significant Trend
	November	0.299	0.014	4.012	Significant Trend
	December	0.364	0.003	5.905	Significant Trend
Kanthalai Tank	February	0.259	0.041	2.085	Significant Trend
	February	0.287	0.017	7.254	Significant Trend
Kaudulla Wewa	June	0.480	<0.0001	2.343	Significant Trend
	July	0.383	0.001	2.264	Significant Trend
	August	0.340	0.005	2.558	Significant Trend
Kothmale	September	0.257	0.033	1.792	Significant Trend
	November	0.269	0.028	3.435	Significant Trend
Mapakadawewa	June	−0.265	0.030	−1.874	Significant Trend
	July	−0.242	0.047	−1.979	Significant Trend
	September	−0.280	0.022	−2.184	Significant Trend
	November	0.280	0.022	3.393	Significant Trend
	December	0.299	0.014	5.105	Significant Trend

Table 6: Continued.

Observed data					
Station	Month	Kendall's Tau	*P* value (two-tailed)	Sen's slope (mm/month)	Remark
Parakramasamudraya	June	−0.250	0.034	−1.209	Significant Trend
	July	−0.247	0.037	−1.463	Significant Trend
	September	−0.331	0.005	−2.288	Significant Trend
Polgolla	March	0.255	0.048	3.045	Significant Trend
	July	−0.320	0.011	−1.998	Significant Trend
	December	0.264	0.040	3.727	Significant Trend
IMERG					
Station	Month	Kendall's Tau	*P* value (two-tailed)	Sen's slope (mm/month)	Remark
Angamedilla	May	0.368	0.039	6.495	Significant Trend
Kothmale	May	0.412	0.017	7.677	Significant Trend
Nawalapitiya	May	0.353	0.048	6.468	Significant Trend
Nuwaraeliya	January	−0.392	0.019	−6.331	Significant Trend
Polgolla	May	0.438	0.011	6.920	Significant Trend
TRMM-3B42					
Station	Month	Kendall's Tau	*P* value (two-tailed)	Sen's slope (mm/month)	Remark
Ambewala	October	0.373	0.031	6.604	Significant Trend
Angamedilla	June	−0.389	0.016	−4.339	Significant Trend
Bandarawela	October	0.373	0.031	6.604	Significant Trend
Giritale	June	−0.413	0.014	−2.258	Significant Trend
Illukumbura	June	−0.386	0.025	−4.779	Significant Trend
Kanthalai Tank	August	0.352	0.025	3.946	Significant Trend
Katugasthota	January	−0.316	0.040	−5.565	Significant Trend
Kaudulla Wewa	June	−0.387	0.018	−2.105	Significant Trend
Nuwaraeliya	January	−0.307	0.045	−4.132	Significant Trend
Parakramasamudraya	March	0.324	0.040	2.976	Significant Trend
Polgolla	May	0.314	0.046	6.070	Significant Trend
TRMM-3B42RT					
Station	Month	Kendall's Tau	*P* value (two-tailed)	Sen's slope (mm/month)	Remark
Angamedilla	April	−0.415	0.013	−9.658	Significant Trend
	June	−0.373	0.031	−3.975	Significant Trend
Giritale	June	−0.439	0.015	−2.791	Significant Trend
Illukumbura	August	0.383	0.038	4.155	Significant Trend
Kanthalai Tank	April	−0.450	0.007	−4.802	Significant Trend
Kaudulla Wewa	April	−0.359	0.037	−7.386	Significant Trend
	June	−0.409	0.019	−2.120	Significant Trend
Kothmale	May	0.450	0.007	9.803	Significant Trend
Mapakadawewa	August	0.500	0.007	7.515	Significant Trend
Nawalapitiya	May	0.386	0.025	7.939	Significant Trend
Nuwaraeliya	February	0.357	0.033	6.566	Significant Trend
Parakramasamudraya	April	−0.427	0.011	−6.898	Significant Trend
	August	0.345	0.039	5.001	Significant Trend
Polgolla	May	0.450	0.007	12.377	Significant Trend

3.4.1. Mann-Kendall Test. The MK test that was performed for monthly, seasonal, and annual time scales of the observed rainfall gauge data showed significant increasing trends mostly in the intermediate zone of the river basin. Increasing trends in the seasonal analysis were mostly in the second intermonsoon season. In the annual and monthly analysis, the wet zone also showed significant increasing trends similar to the finding of Pawar and Rathnayake [83]. IMERG product agreed more with the trends observed in the rainfall gauge data in the monthly and annual time scales. TRMM-3B42 showed significant increasing trends during the second intermonsoon in the intermediate zone. In TRMM-3B42 and PERSIANN-CDR, from the monthly analysis, negative significant trends (dry zone) were mostly observed. In all three time scales, PERSIANN-CCS showed increasing trends in the wet zone. However, PERSIANN-CDR and TRMM-3B42RT showed mixed results while PERSIANN showed no significant trends in all three time scales.

3.4.2. Sen's Slope Estimator Test. Sen's slope for the trends obtained from the MK test indicated a slope >1.5 mm/month in the monthly analysis for the observed data. For the annual and seasonal analysis, the slopes were >20 mm/year and >9 mm/season, respectively. In the monthly analysis, IMERG indicated an increasing trend of >6 mm/month. High intensity increasing trends of >30 mm/year in the annual time scale were observed in IMERG and both TRMM

Table 7: Seasonal analysis of MK test and Sen's slope estimator significant trend results.

Observed Data					
Station	Season	Kendall's Tau	*P* value (two-tailed)	Sen's slope (mm/season)	Remark
Illukumbura	SIM	0.273	**0.026**	9.941	Significant Trend
Mapakadawewa	SIM	0.265	**0.030**	11.116	Significant Trend
Nawalapitiya	FIM	0.328	**0.014**	7.904	Significant Trend
	NEM	0.512	**<0.0001**	15.453	Significant Trend
Nuwaraeliya	SIM	0.297	**0.021**	7.056	Significant Trend
PERSIANN					
Station	Season	Kendall's Tau	*P* value (two-tailed)	Sen's slope (mm/season)	Remark
Kaudulla Wewa	FIM	−0.359	**0.037**	−14.233	Significant Trend
Parakramasamudraya	FIM	−0.345	**0.039**	−9.185	Significant Trend
PERSIANN-CCS					
Station	Season	Kendall's Tau	*P* value (two-tailed)	Sen's alope (mm/season)	Remark
Illukumbura	NEM	0.462	**0.028**	24.222	Significant Trend
Katugasthota	SWM	0.412	**0.021**	38.830	Significant Trend
Kothmale	SWM	0.567	**0.002**	35.542	Significant Trend
Mapakadawewa	SIM	0.436	**0.038**	27.250	Significant Trend
Parakramasamudraya	FIM	−0.367	**0.048**	−17.655	Significant Trend
Polgolla	SWM	0.483	**0.01**	47.500	Significant Trend
PERSIANN-CDR					
Station	Season	Kendall's Tau	*P* value (two-tailed)	Sen's slope (mm/season)	Remark
Ambewala	SWM	−0.246	**0.044**	−4.993	Significant Trend
Angamedilla	SIM	0.257	**0.030**	5.424	Significant Trend
	SWM	−0.287	**0.015**	−5.377	Significant Trend
Giritale	SIM	0.291	**0.016**	5.651	Significant Trend
	SWM	−0.262	**0.029**	−4.768	Significant Trend
	NEM	0.367	**0.010**	8.769	Significant Trend
Illukumbura	SIM	0.299	**0.014**	6.994	Significant Trend
	SWM	−0.428	**0.010**	−9.474	No Trend
Kanthalai Tank	NEM	0.290	**0.020**	9.922	Significant Trend
Kaudulla Wewa	NEM	0.375	**0.010**	13.545	Significant Trend
	SIM	0.355	**0.010**	8.153	Significant Trend
	SWM	0.550	**<0.0001**	11.862	Significant Trend
Mapakadawewa	SIM	0.242	**0.047**	5.474	Significant Trend
	SWM	−0.430	**0.010**	−8.966	Significant Trend
Nawalapitiya	NEM	0.266	**0.043**	7.347	Significant Trend
Parakramasamudraya	SIM	0.247	**0.037**	4.514	Significant Trend
	SWM	−0.247	**0.037**	−4.964	Significant Trend
Polgolla	NEM	0.260	**0.040**	8.054	Significant Trend
IMERG					
Station	Season	Kendall's Tau	*P* value (two-tailed)	Sen's slope (mm/season)	Remark
Katugasthota	SWM	0.368	**0.023**	10.622	Significant Trend
Kothmale	SWM	0.404	**0.016**	14.497	Significant Trend
Nawalapitiya	SWM	0.346	**0.045**	12.768	Significant Trend
Polgolla	SWM	0.357	**0.033**	12.283	Significant Trend
TRMM-3B42					
Station	Season	Kendall's Tau	*P* value (two-tailed)	Sen's slope (mm/season)	Remark
Ambewala	FIM	0.399	**0.021**	9.543	Significant Trend
	SIM	0.359	**0.037**	12.752	Significant Trend
Bandarawela	SIM	0.359	**0.037**	12.752	Significant Trend
Illukumbura	FIM	0.359	**0.037**	7.277	Significant Trend
	SIM	0.359	**0.037**	16.176	Significant Trend
Mapakadawewa	SIM	0.359	**0.037**	12.259	Significant Trend
TRMM-3B42RT					
Station	Season	Kendall's Tau	*P* value (two-tailed)	Sen's slope (mm/season)	Remark
Ambewala	SIM	0.417	**0.024**	19.470	Significant Trend
Bandarawela	SIM	0.417	**0.024**	19.470	Significant Trend
Illukumbura	NEM	0.483	**0.009**	39.989	Significant Trend
Kanthalai Tank	FIM	−0.368	**0.028**	−4.435	Significant Trend

Table 7: Continued.

Observed Data					
Station	Season	Kendall's Tau	*P* value (two-tailed)	Sen's slope (mm/season)	Remark
Kothmale	SWM	0.415	**0.013**	20.820	Significant Trend
Nawalapitiya	SWM	0.346	**0.045**	18.558	Significant Trend
Parakramasamudraya	SWM	0.415	**0.013**	18.072	Significant Trend

products. TRMM-3B42 showed increasing trends of >12 mm/season during the second intermonsoon season in the intermediate zone. The increasing trends shown by PERSIANN-CCS were >10 mm/year in the annual analysis. Figure 10 demonstrates the MK and Sen's slope estimator results obtained for the annual time scale. The results of the significant trends in the monthly and seasonal analysis are attached in Tables 6 and 7.

From the nonparametric analysis, the results concluded that the IMERG product agrees more with RG data in monthly and annual time scales while TRMM-3B42 agrees more in the seasonal analysis. These findings agree with a recent study by Hussein et al. [84]. Therefore, depending on these results, a careful choice of products for the different zones in the river basin is required. This showed that even in the same river basin, products behave differently with trend patterns depending on the climatic seasons and zones of the river basin.

4. Conclusions

In this research study, six SRPs (PERSIANN, PERSINN-CCS, PERSIANN-CDR, IMERG, TRMM-3B42, and TRMM-3B42RT) were evaluated against rainfall gauge data. Observed data at 14 locations spatially distributed in the three climatic zones of the MRB, Sri Lanka, were selected. Four categorical indices, FAR, POD, CSI, and PC, were used to determine the accuracy of rainfall detection and prediction of satellite products during light and heavy rainfall. IMERG product showed better performance while PERSIANN-CDR showed the worst performance in detecting and predicting rainfall during both these rainfall events. The accuracy of the SRPs was also evaluated using five continuous evaluation indices, CC, RMSE, MAE, RB, and KGE. Among the six evaluated products, in general, IMERG showed better performance while PERSIANN products showed poor performance. However, IMERG also caused underestimations of rainfall data. From the performance shown in all the continuous evaluation indices, all products cannot efficiently reproduce the temporal variability of RG data in both daily and monthly time scales. From the nonparametric tests done on the two datasets SRP and observed rainfall data to identify any significant trends, it was concluded that the IMERG product agrees more with observed rainfall data in monthly and annual time scales while TRMM-3B42 agrees more on the seasonal scale. In all three time scales, PERSIANN-CCS showed increasing trends in the wet zone. However, altogether, PERSIANN-CDR and TRMM-3B42RT showed mixed results while PERSIANN showed no significant trends in all three time scales. It can be concluded that a careful selection of global precipitation products is required prior to using them in any application. This showed that even in the same river basin, products behave differently with trend patterns depending on the climatic seasons and zones of the river basin. It was also clear that these products possess significant errors which cannot be ignored when using them in hydrological applications. However, in places of scarce rainfall data in the MRB, IMERG product proved to be a better choice overall. This study being the first of a kind that incorporated SRPs and observed rainfall data for the Mahaweli River Basin, Sri Lanka, is an immense contribution to many stakeholders and the research community as this basin carries significant importance to the country. This research study was subjected to limitations with the use of six research-based SRPs and 14 rain gauge stations. Therefore, further, it is recommended to carry out studies incorporating near-real-time products with more rain gauge stations to avoid point-pixel errors.

Data Availability

The climatic data used in this research study are available upon request for research purposes.

Conflicts of Interest

The authors declare no conflicts of interest.

Acknowledgments

The authors of this manuscript are grateful to all SRP communities for making the precipitation data freely available to the international research community. In addition, the authors would like to thank Mr. Jayanga Samarasinghe from Sri Lanka Institute of Information Technology, Sri Lanka, and Ms. Pavithra K. Baddewela from Transport and Logistic Management, University of Moratuwa, Sri Lanka, for their support in writing this paper. This research received no external funding.

References

[1] M. D. A. Qizi, *Water Resources and their Use in The National Economy*, Builders Of The Future, 2021.

[2] R. Loritz, M. Hrachowitz, M. Neuper, and E. Zehe, "The role and value of distributed precipitation data in hydrological models," *Hydrology and Earth System Sciences*, vol. 25, no. 1, pp. 147–167, 2021.

[3] R. Roca, L. V. Alexander, G. Potter et al., "FROGS: a daily $1^{\circ} \times 1^{\circ}$ gridded precipitation database of rain gauge, satellite and reanalysis products," *Earth System Science Data*, vol. 11, no. 3, pp. 1017–1035, 2019.

[4] E. C. Barrett, "Precipitation measurement by satellites: towards community algorithms," *Advances in Space Research*, vol. 13, no. 5, pp. 119–136, 1993.

[5] L. Brocca, P. Filippucci, S. Hahn et al., "SM2RAIN-ASCAT (2007-2018): global daily satellite rainfall data from ASCAT

soil moisture observations," *Earth System Science Data*, vol. 11, no. 4, pp. 1583–1601, 2019.

[6] M. B. Gunathilake, Y. V. Amaratunga, A. Perera, C. Karunanayake, A. S. Gunathilake, and U. Rathnayake, "Statistical evaluation and hydrologic simulation capacity of different satellite-based precipitation products (SbPPs) in the Upper Nan River Basin, Northern Thailand," *Journal of Hydrology: Regional Studies*, vol. 32, Article ID 100743, 2020.

[7] G. J. Ciach, "Local random errors in tipping-bucket rain gauge measurements," *Journal of Atmospheric and Oceanic Technology*, vol. 20, no. 5, pp. 752–759, 2003.

[8] G. Villarini, P. Mandapaka, W. Krajewski, and R. Moore, "Rainfall and sampling uncertainties: a rain gauge perspective," *Journal of Geophysical Research*, vol. 113, 2008.

[9] C. Karunanayake, M. B. Gunathilake, and U. Rathnayake, "Inflow forecast of iranamadu reservoir, Sri lanka, under projected climate scenarios using artificial neural networks," *Applied Computational Intelligence and Soft Computing*, vol. 2020, Article ID 8821627, 11 pages, 2020.

[10] K. E. Trenberth, A. Dai, R. M. Rasmussen, and D. B. Parsons, "The changing character of precipitation," *Bulletin of the American Meteorological Society*, vol. 84, no. 9, pp. 1205–1218, 2003.

[11] J. Shi, F. Yuan, C. Shi et al., "Statistical evaluation of the latest GPM-Era IMERG and GSMaP satellite precipitation products in the Yellow River source region," *Water*, vol. 12, no. 4, p. 1006, 2020.

[12] G. J. Huffman, D. T. Bolvin, E. J. Nelkin et al., "The TRMM Multisatellite Precipitation Analysis (TMPA): quasi-global, multiyear, combined-sensor precipitation estimates at fine scales," *Journal of Hydrometeorology*, vol. 8, no. 1, pp. 38–55, 2007.

[13] R. Joyce, J. Janowiak, P. Arkin, and P. Xie, "CMORPH: a method that produces global precipitation estimates from passive microwave and infrared data at high spatial and temporal resolution," *Journal of Hydrometeorology*, vol. 5, no. 3, pp. 487–503, 2004.

[14] S. Sorooshian, K.-L. Hsu, X. Gao, H. V. Gupta, B. Imam, and D. Braithwaite, "Evaluation of PERSIANN system satellite-based estimates of tropical rainfall," *Bulletin of the American Meteorological Society*, vol. 81, no. 9, pp. 2035–2046, 2000.

[15] H. E. Beck, A. I. J. M. Van Dijk, V. Levizzani et al., "MSWEP: 3-hourly 0.25° global gridded precipitation (1979–2015) by merging gauge, satellite, and reanalysis data," *Hydrology and Earth System Sciences*, vol. 21, no. 1, pp. 589–615, 2017.

[16] M. M. Bitew and M. Gebremichael, "Evaluation through independent measurements: complex terrain and humid tropical region in Ethiopia," *Satellite Rainfall Applications for Surface Hydrology*, Spriger, Berlin, Germany, pp. 205–214, 2009.

[17] E. N. Anagnostou, V. Maggioni, E. I. Nikolopoulos, T. Meskele, F. Hossain, and A. Papadopoulos, "Benchmarking high-resolution global satellite rainfall products to radar and rain-gauge rainfall estimates," *IEEE Transactions on Geoscience and Remote Sensing*, vol. 48, no. 4, pp. 1667–1683, 2010.

[18] S. Jiang, L. Ren, B. Yong, X. Yang, and L. Shi, "Evaluation of high-resolution satellite precipitation products with surface rain gauge observations from laohahe basin in Northern China," *Water Science and Engineering*, vol. 3, 2010.

[19] A. Mondal, V. Lakshmi, and H. Hashemi, "Intercomparison of trend analysis of multisatellite monthly precipitation products and gauge measurements for river basins of India," *Journal of Hydrology*, vol. 565, pp. 779–790, 2018.

[20] M. B. Gunathilake, M. Zamri, T. P. Alagiywanna et al., "Hydrologic utility of satellite-based and gauge-based gridded precipitation products in the Huai Bang Sai Watershed of Northeastern Thailand," *Hydrology*, vol. 8, no. 4–165, pp. 1–21, 2021.

[21] P. Xie and P. A. Arkin, "Analyses of global monthly precipitation using gauge observations, satellite estimates, and numerical model predictions," *Journal of Climate*, vol. 9, no. 4, pp. 840–858, 1996.

[22] A. V. Mehta and S. Yang, "Precipitation climatology over Mediterranean Basin from ten years of TRMM measurements," *Advances in Geosciences*, vol. 17, pp. 87–91, 2008.

[23] A. Milewski, R. Elkadiri, and M. Durham, "Assessment and comparison of TMPA satellite precipitation products in varying climatic and topographic regimes in Morocco," *Remote Sensing*, vol. 7, no. 5, pp. 5697–5717, 2015.

[24] K. Tong, F. Su, D. Yang, and Z. Hao, "Evaluation of satellite precipitation retrievals and their potential utilities in hydrologic modeling over the Tibetan Plateau," *Journal of Hydrology*, vol. 519, pp. 423–437, 2014.

[25] B. Kumar, K. C. Patra, and V. Lakshmi, "Daily rainfall statistics of TRMM and CMORPH: a case for trans-boundary Gandak river basin," *Journal of Earth System Science*, vol. 125, no. 5, pp. 919–934, 2016.

[26] S. Prakash, A. K. Mitra, D. S. Pai, and A. AghaKouchak, "From TRMM to GPM: how well can heavy rainfall be detected from space?" *Advances in Water Resources*, vol. 88, pp. 1–7, 2016.

[27] F. Fatkhuroyan, T. Wati, A. Sukmana, and R. Kurniawan, "Validation of satellite daily rainfall estimates over Indonesia," *Forum Geografi*, vol. 32, no. 2, pp. 170–180, 2018.

[28] S. Yoshimoto and G. Amarnath, "Applications of satellite-based rainfall estimates in flood inundation modeling-A case study in Mundeni Aru river basin, Sri Lanka," *Remote Sensing*, vol. 9, no. 10, p. 998, 2017.

[29] M. B. Gunathilake, C. Karunanayake, A. S. Gunathilake et al., "Hydrological models and artificial neural networks (ANNs) to simulate streamflow in a tropical catchment of Sri Lanka," *Applied Computational Intelligence and Soft Computing*, vol. 2021, Article ID 6683389, 9 pages, 2021.

[30] M. B. Gunathilake, T. Senerath, T. Senerath, and U. Rathnayake, "Artificial neural network based PERSIANN data sets in evaluation of hydrologic utility of precipitation estimations in a tropical watershed of Sri Lanka," *AIMS Geosciences*, vol. 7, no. 3, pp. 478–489, 2021.

[31] L. Zubair, "El Niño-southern oscillation influences on the Mahaweli streamflow in Sri Lanka," *International Journal of Climatology*, vol. 23, no. 1, pp. 91–102, 2003.

[32] S. Diyabalanage, S. Abekoon, I. Watanabe et al., "Has irrigated water from Mahaweli river contributed to the kidney disease of uncertain etiology in the dry zone of Sri Lanka?" *Environmental Geochemistry and Health*, vol. 38, no. 3, pp. 679–690, 2016.

[33] H. Selvarajah, T. Koike, M. Rasmy et al., "Development of an integrated approach for the assessment of climate change impacts on the hydro-meteorological characteristics of the Mahaweli river basin, Sri Lanka," *Water*, vol. 13, no. 9, p. 1218, 2021.

[34] S. Withanachchi, S. Köpke, C. Withanachchi, R. Pathiranage, and A. Ploeger, "Water resource management in dry zonal paddy cultivation in Mahaweli River basin, Sri Lanka: an analysis of spatial and temporal climate change impacts and traditional knowledge," *Climate*, vol. 2, no. 4, pp. 329–354, 2014.

[35] S. Shelton and Z. Lin, "Streamflow variability in Mahaweli River basin of Sri Lanka during 1990-2014 and its possible mechanisms," *Water*, vol. 11, no. 12, p. 2485, 2019.

[36] Z. Lin and S. Shelton, "Interdecadal change of drought characteristics in Mahaweli river basin of Sri Lanka and the associated atmospheric circulation difference," *Frontiers of Earth Science*, vol. 8, 2020.

[37] N. Imbulana, S. Gunawardana, S. Shrestha, and A. Datta, "Projections of extreme precipitation events under climate change scenarios in Mahaweli river basin of Sri Lanka," *Current Science*, vol. 114, no. 07, pp. 1495–1509, 2018.

[38] T. R. W. S. Dhanapala and H. A. H. Jayasena, "Hydrologic model for selected sub-catchments in the Mahaweli basin of Sri Lanka," in *Proceedings of the National Conference on Status and Future Direction of Water Research in Sri Lanka*, vol. 17, International Water Management Institute, Colombo, Sri Lanka, 1998.

[39] U. Rathnayake, S. B. Weerakoon, K. D. W. Nandalal, and U. Rathnayake, "Flood modeling in the Mahaweli river reach from kothmale to polgolla," *International conference on Mitigation of the risk of natural hazards, Peradeniya, Sri Lanka*, vol. 8, 2007.

[40] E. P. N. Udayakumara and U. A. D. P. Gunawardena, *Reducing Siltation and Increasing Hydropower Generation from the Rantambe Reservoir, Sri Lanka*, South Asian Network for Development and Environmental Economics (SANDEE), Paper, Kathmandu, Nepal, 2016.

[41] B. A. R. H. Dias, E. P. N. Udayakumara, J. M. C. K. Jayawardana, S. Malavipathirana, and D. A. T. W. K. Dissanayake, "Assessment of soil erosion in uma oya catchment, Sri Lanka," *Journal of Environmental Professionals Sri Lanka*, vol. 8, no. 1, 2019.

[42] H. Gunatilake and G. Vieth, "Estimation of on-site cost of soil erosion: a comparison of replacement and productivity change methods," *Journal of Soil and Water Conservation*, vol. 55, pp. 197–204, 2000.

[43] T. Hewawasam, "Effect of land use in the upper Mahaweli catchment area on erosion, landslides and siltation in hydropower reservoirs of Sri Lanka," *Journal of the National Science Foundation of Sri Lanka*, vol. 38, no. 1, 2010.

[44] J. M. C. K. Jayawardana, W. D. T. M. Gunawardana, E. P. N. Udayakumara, and M. Westbrooke, "Land use impacts on river health of Uma Oya, Sri Lanka: implications of spatial scales," *Environmental Monitoring and Assessment*, vol. 189, no. 4, p. 192, 2017.

[45] R. N. N. Weerasinghe, J. M. C. K. Jayawardana, and E. P. N. Udayakumara, "Quantitative assessment of soil erosion and its association with river health in Uma Oya watershed in Sri Lanka," in *Proceedings of the ISAE 2016*, pp. 137–140, Niagara-On-The-Lake, Canada, October 2016.

[46] P. Aravinna, N. Priyantha, A. Pitawala, and S. K. Yatigammana, "Use pattern of pesticides and their predicted mobility into shallow groundwater and surface water bodies of paddy lands in Mahaweli river basin in Sri Lanka," *Journal of Environmental Science and Health, Part B*, vol. 52, no. 1, pp. 37–47, 2016.

[47] C. B. Dissanayake and S. V. R. Weerasooriya, "The environmental chemistry of Mahaweli river, Sri Lanka," *International Journal of Environmental Studies*, vol. 28, pp. 207–223, 1986.

[48] B. A. Malmgren, R. Hulugalla, Y. Hayashi, and T. Mikami, "Precipitation trends in Sri Lanka since the 1870s and relationships to El Niño-southern oscillation," *International Journal of Climatology*, vol. 23, no. 10, pp. 1235–1252, 2003.

[49] J. M. R. S. Bandara, H. V. P. Wijewardena, Y. M. A. Y. Bandara, R. G. P. T. Jayasooriya, and H. Rajapaksha, "Pollution of river mahaweli and farmlands under irrigation by cadmium from agricultural inputs leading to a chronic renal failure epidemic among farmers in NCP, Sri Lanka," *Environmental Geochemistry and Health*, vol. 33, no. 5, pp. 439–453, 2011.

[50] Y. Mu, T. Biggs, and S. S. P. Shen, "Satellite-based precipitation estimates using a dense rain gauge network over the southwestern brazilian amazon: implication for identifying trends in dry season rainfall," *Atmospheric Research*, vol. 261, Article ID 105741, 2021.

[51] V. H. D. M. Paca, G. Espinoza-Dávalos, D. Moreira, and G. Comair, "Variability of trends in precipitation across the amazon river basin determined from the CHIRPS precipitation product and from station records," *Water*, vol. 12, no. 5, p. 1244, 2020.

[52] R. B. L. Cavalcante, D. B. d. S. Ferreira, P. R. M. Pontes, R. G. Tedeschi, C. P. W. da Costa, and E. B. de Souza, "Evaluation of extreme rainfall indices from CHIRPS precipitation estimates over the Brazilian Amazonia," *Atmospheric Research*, vol. 238, Article ID 104879, 2020.

[53] G. J. Huffman, R. F. Adler, D. T. Bolvin, and E. J. Nelkin, "The TRMM multi-satellite precipitation analysis (TMPA)," in *Satellite Rainfall Applications for Surface Hydrology*, pp. 3–22, Springer, Dordrecht, Netherlands, 2010.

[54] G. J. Huffman, D. T. Bolvin, D. Braithwaite et al., *Algorithm Theoretical Basis Document (Atbd) Version 06 Nasa Global Precipitation Measurement (Gpm) Integrated Multi-Satellite Retrievals for Gpm (Imerg)*, National Aeronautics and Space Administration, Washington, DC, USA, 2019.

[55] G. J. Huffman, *NASA Global Precipitation Measurement (GPM) Integrated Multi Satellite Retrievals for GPM (IMERG)*, NASA, Washington, DC, USA, 2020.

[56] M. Alijanian, G. R. Rakhshandehroo, A. K. Mishra, and M. Dehghani, "Evaluation of satellite rainfall climatology using CMORPH, PERSIANN-CDR, PERSIANN, TRMM, MSWEP over Iran," *International Journal of Climatology*, vol. 37, no. 14, pp. 4896–4914, 2017.

[57] K.-L. Hsu, A. Behrangi, B. Imam, and S. Sorooshian, "Extreme precipitation estimation using satellite-based PERSIANN-CCS algorithm," in *Satellite Rainfall Applications for Surface Hydrology*, pp. 49–67, Springer, Dordrecht, Netherlands, 2010.

[58] Y. Hong, D. Gochis, J.-t. Cheng, K.-l. Hsu, and S. Sorooshian, "Evaluation of PERSIANN-CCS rainfall measurement using the NAME event rain gauge network," *Journal of Hydrometeorology*, vol. 8, no. 3, pp. 469–482, 2007.

[59] H. Ashouri, K.-L. Hsu, S. Sorooshian et al., "PERSIANN-CDR: daily precipitation climate data record from multisatellite observations for hydrological and climate studies," *Bulletin of the American Meteorological Society*, vol. 96, no. 1, pp. 69–83, 2015.

[60] F. Gadouali and M. Messouli, "Evaluation of multiple satellite-derived rainfall products over Morocco," *International Journal of Horticultural Science and Technology*, vol. 10, no. 1, pp. 72–89, 2020.

[61] M. N. Anjum, Y. Ding, D. Shangguan, M. W. Ijaz, and S. Zhang, "Evaluation of high-resolution satellite-based real-time and post-real-time precipitation estimates during 2010 extreme flood event in swat river basin, hindukush region," *Advances in Meteorology*, vol. 2016, Article ID 2604980, 8 pages, 2016.

[62] M. S. Nashwan, S. Shahid, and X. Wang, "Assessment of satellite-based precipitation measurement products over the hot desert climate of Egypt," *Remote Sensing*, vol. 11, no. 5, p. 555, 2019.

[63] A. B. Ayub, F. Tangang, L. Juneng, M. L. Tan, and J. X. Chung, "Evaluation of gridded precipitation data sets in Malaysia," *Remote Sensing*, vol. 12, no. 4, p. 613, 2020.

[64] G. Wei, H. Lü, W. T Crow, Y. Zhu, J. Wang, and J. Su, "Evaluation of satellite-based precipitation products from IMERG V04A and V03D, CMORPH and TMPA with gauged rainfall in three climatologic zones in China," *Remote Sensing*, vol. 10, no. 1, p. 30, 2018.

[65] F. Chen and X. Li, "Evaluation of IMERG and TRMM 3B43 monthly precipitation products over mainland China," *Remote Sensing*, vol. 8, no. 6, p. 472, 2016.

[66] H. V. Gupta, H. Kling, K. K. Yilmaz, and G. F. Martinez, "Decomposition of the mean squared error and NSE performance criteria: implications for improving hydrological modelling," *Journal of Hydrology*, vol. 377, no. 1-2, pp. 80–91, 2009.

[67] H. Kling, M. Fuchs, and M. Paulin, "Runoff conditions in the upper Danube basin under an ensemble of climate change scenarios," *Journal of Hydrology*, vol. 424-425, pp. 264–277, 2012.

[68] D. E. Radcliffe and R. Mukundan, "PRISMvs. CFSR precipitation data effects on calibration and validation of SWAT models," *Journal of the American Water Resources Association*, vol. 53, no. 1, pp. 89–100, 2017.

[69] H. Akoglu, "User's guide to correlation coefficients," *Turkish journal of emergency medicine*, vol. 18, no. 3, pp. 91–93, 2018.

[70] H. B. Mann, "Nonparametric tests against trend," *Journal of the econometric society*, vol. 13, no. 3, pp. 245–259, 1945.

[71] M. G. Kendall, *Rank Correlation Methods*, Griffin, London, UK, 4th edition, 1948.

[72] HydroGeoLogic Inc, *Final 2004 Annual Groundwater Monitoring Report and Quarterly Groundwater Monitoring Report, Quarter 4, 2004, Operable Unit 1 Fritzsche Army Airfield Fire Drill Area Former fort Ord California*, HydroGeoLogic Inc, Huntsville, AL, USA, 2005.

[73] S. I. Sridhar and A. Raviraj, "Statistical trend analysis of rainfall in Amaravathi river basin using Mann-Kendall test," *Current World Environment*, vol. 12, no. 1, pp. 89–96, 2017.

[74] S. Moazami and M. R. Najafi, "A comprehensive evaluation of GPM-IMERG V06 and MRMS with hourly ground-based precipitation observations across Canada," *Journal of Hydrology*, vol. 594, Article ID 125929, 2021.

[75] C. Yu, D. Hu, Y. Di, and Y. Wang, "Performance evaluation of IMERG precipitation products during typhoon Lekima (2019)," *Journal of Hydrology*, vol. 597, Article ID 126307, 2021.

[76] M. Amjad, M. T. Yilmaz, I. Yucel, and K. K. Yilmaz, "Performance evaluation of satellite- and model-based precipitation products over varying climate and complex topography," *Journal of Hydrology*, vol. 584, Article ID 124707, 2020.

[77] M. Dembélé and S. J. Zwart, "Evaluation and comparison of satellite-based rainfall products in burkina faso, West Africa," *International Journal of Remote Sensing*, vol. 37, no. 17, pp. 3995–4014, 2016.

[78] G. B. Adane, B. A. Hirpa, C.-H. Lim, and W.-K. Lee, "Evaluation and comparison of satellite-derived estimates of rainfall in the diverse climate and terrain of central and northeastern Ethiopia," *Remote Sensing*, vol. 13, no. 7, p. 1275, 2021.

[79] M. Masood, A. S. Shakir, A. H. Azhar, G. Nabi, and fnm Habib-u-Rehman, "Assessment of real time, multi-satellite precipitation products under diverse climatic and topographic conditions," *Asia-Pacific Journal of Atmospheric Sciences*, vol. 56, no. 4, pp. 577–591, 2020.

[80] M. N. Anjum, Y. Ding, D. Shangguan et al., "Performance evaluation of latest integrated multi-satellite retrievals for global precipitation measurement (IMERG) over the northern highlands of Pakistan," *Atmospheric Research*, vol. 205, pp. 134–146, 2018.

[81] M. Yang, Z. Li, M. N. Anjum, and Y. Gao, "Performance evaluation of version 5 (V05) of integrated multi-satellite retrievals for global precipitation measurement (IMERG) over the tianshan Mountains of China," *Water*, vol. 11, no. 6, p. 1139, 2019.

[82] M. T. Mahmoud, M. A. Al-Zahrani, and H. O. Sharif, "Assessment of global precipitation measurement satellite products over Saudi Arabia," *Journal of Hydrology*, vol. 559, pp. 1–12, 2018.

[83] U. Pawar and U. Rathnayake, "Spatiotemporal rainfall variability and trend analysis over mahaweli basin, Sri Lanka," *Arabian Journal of Geosciences*, vol. 15, no. 320, pp. 1–16, 2022.

[84] K. A. Hussein, T. S. Alsumaiti, D. T. Ghebreyesus, H. O. Sharif, and W. Abdalati, "High-resolution spatiotemporal trend analysis of precipitation using satellite-based products over the United Arab Emirates," *Water*, vol. 13, no. 17, p. 2376, 2021.